Table IV: Proposed and Actual Activity for Subproject 4.

| Months Mo | Months | Months | Months | Months | (←→) | : Proposed | ctivit |
|-------------|--|-----------------------|-----------------------|-----------------------|-------------------------|-----------------|--------|
| 25-30 31 | 19-24 | 13-18 | 7-12 | 1-6 | (\longleftrightarrow) | Actual | |
| - | | | | <> | e: statistical | rch literature | . Se |
| | | | | \longleftrightarrow | | hods | me |
| | | | | | lence | t of independ | Te |
| | | | | | al log-linear | o-dimensiona | Tv |
| | | | | | | dels | mo |
| | | | | | nal log- | ee-dimensior | , Th |
| | | | | | | ar models | lin |
| | | } | | | ion models | istic regressi | i Lo |
| | | | <> | | | a collection. | . · Da |
| | | | \longleftrightarrow | | | | ! |
| . — | < | | | | | gress report. | . Pr |
| | $\stackrel{\widehat{\longleftarrow}}{\longleftrightarrow}$ | | | | | | ı |
| | | | | | lence | t of independ | . Te |
| | | \longleftrightarrow | | | ncer | ween two can | be |
| | | | | | | ables. | va |
| | | ~ | | | wo | olication of tw | . Ај |
| | | ←> | | | -linear | ensional log- | di |
| | | | | | | dels. | mo |
| | | ~ | | | hree | olication of th | . A |
| | | \longleftrightarrow | | | -linear | ensional log- | di |
| | | | | | | dels. | me |
| | | | | | ogistic | olication of lo | . Ap |
| | <u>-</u> | | | | els | ression mode | re |
| | | l | | | port | l progress rep | . Fu |
| ← | | | | | | Ì | ! |
| | < | | | | els | plication of lo | . Ap |

Outputs of Subproject 4

Papers presented in international conferences

3

Master graduates

3

Subproject 5: Modeling and Computer Simulation in Cancer
Research: Theory and Modeling of the Growth of
Tumors

Principal Investigator: Asst. Prof. Dr. Wannapong Triampo

Proposed activities

We now have completed our work on the stochastic cellular automata *in silico* model for immune system- avascular tumor interactions *in vivo*: self-organized vascular growth, pattern formation and fractal analysis. Also the final draft of the manuscript is about to be finished and is expected to be submitted in a few weeks. It can be summarized as follows. The stochastic discrete model on two-dimensional square lattice has been developed. The cellular automata method was presented to describe the growth of an avascular tumor based on microscopic scale of immune system response, cell proliferation, cell death and degradation. The Monte-Carlo method was applied in this model which enables us to idealize three regimes of Gompertzian growth. We have used scaling techniques to analyze the fractality of tumor colony, proliferating tumor colony as well as statistical properties to make conclusions about the fractality of the boundary.

5.1 The model

5.1.1 The microscopic scale

The basic biological principles, which is represented by the microscopic scale change, are cell proliferation as well as its interaction with the immune system as shown in Fig. 5.1.

It is established that the immune system has an important role which influences the development of avascular tumor growth. The immune system is very complicated. Let us consider a simplified process of a growing avascular tumor which effects an immune response in the host immune system. By [10, 29 and 31], the tumor can be effectively eliminated by tumor-infiltrating cytotoxic lymphocytes (TICLs). Practically, TICLs may be cytotoxic lymphocytes, natural killer-like cells and/or lymphokine activated killer. TICLs are assumed to interact with the tumor cell and then lymphocyte-tumor cell complexes are formed. These lymphocyte-tumor cells complexes detachment results in either the death of tumor cells by a program of lysis or by TICLs without damaging the proliferating tumor cells.

The host tissue is represented by a lattice of size L x L. And any site has coordinates (x_n, y_n) , where $x_n, y_n = 1, 2, ..., L$. We let the proliferating tumor cells, the dead tumor cells, the cytotoxic lymphocyte, and TICLs-tumor cell complexes be represented by P, D, TICLs, and C, respectively. Then, the kinetics of fundamental feature of tumor development could be represented as in Fig. 5.1.

$$P \xrightarrow{r' prolif.} 2P$$

$$P + TICLs \xrightarrow{r_{binding}} C \xrightarrow{r_{lysis}} D + TICLs$$

$$D \xrightarrow{r_{decay}}$$

Fig. 5.1 Kinetic mechanisms of development of cancer with immune response (modified from [1, 10]).

The parameters r_{prolif} , $r_{binding}$, r_{detach} , r_{lysis} , and r_{decay} are non-negative kinetic constants where r_{prolif} describes the base rate of tumor proliferation. $r_{binding}$ represents the rate of binding of TICLs to tumor cells, r_{detach} is the rate of detachment of TICLs from cancer cell without damaging cells, r_{lysis} is the rate of detachment of TICLs from dead tumor cells, resulting in an irreversible programming of the tumor cells for lysis, and r_{decay} describes dissolution of the dead cancer cells. Additionally, we may define the function r'_{prolif} as an avascular tumor growth rate in vivo, by assuming $r'_{prolif}(t) = r_{prolif}(1 - \frac{p}{K})$, where P(t) denotes the number of proliferating tumor cells, and K denotes the carrying capacity, which can be indicated as the restriction of nutrient for proliferation of cancer cells and/or increasing waste product accumulation indices, decreasing the rate of proliferation of cancer cells [27,28].

We investigated the influences of the parameters on the Gompertz growth curve. By Fig. 5.5 (g), r'_{prolif} decreases with increasing cancer cells, and this function incorporates the fact that the proliferating tumor cells growth depends on the competition for resources among the proliferating tumor cells. These effects are assumed in avascular microscopic tumor growth *in vivo* [17] as illustrated in the first reaction of Fig. 5.1. By the second reaction, the parameter r_{detach} indicates the tumor's potential for escaping the host's

<u>4</u>

3

ť

immune surveillance whereas $r_{binding}$ corresponds to the TICLs' response in a chemotactic manner towards tumor cells and r_{lysis} describes the TICLs' detachment rate of activation from tumor cells, being an irreversible programming of the tumor cells for lysis, and r_{decay} represents the dissolution process in which the dead tumor cells turn into normal tissues and reflects the degraded dead tumor cells.

Table 5.1 Summary of functions and input constant parameters for the model.

Functions in the model

 r'_{prolif} Rate of proliferation of cancer cells (varying with the number of proliferating tumor cells)

Parameters

 r_{prolif} Base rate of proliferation of cancer cells

 $r_{binding}$ Rate of TICLs' binding to the tumor cell to become cell complexes

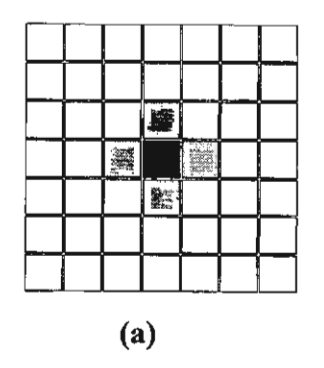
 r_{detach} Rate of TICLs' detachment from the cell complexes without cell damage

 r_{lysis} Rate of TICLs' detachment from the cell complexes resulting in the lysis of tumor cells

 r_{decay} Death rate of tumor cells degrading to normal cells

K The maximum proliferating tumor cells extent

^{*} The parameter values of r_{prolif} , $r_{binding}$, r_{lysis} and r_{decay} have been modified from Qi, et. al. [1], and r_{detach} and r_{lysis} have been modified from Matzavinos, A., et. al [10, 13, 30].



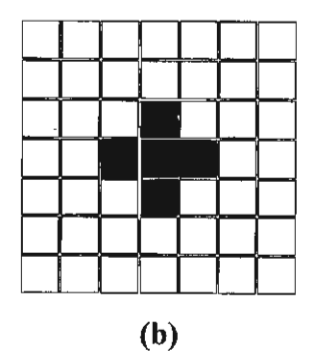


Fig. 5.2 (a) The four nearest neighboring sites (gray) of the tumor site (black): with the nearest neighboring rule of the so-called von Neumann neighborhood.

(b) The initial configuration: five cancer cells in the center of the square lattice.

5.1.2 The methodology for stochastic CA

Time runs in discrete steps. The lattice compartment may accommodate either: proliferating tumor cell (P), TICLs-tumor cell complexes (C), or dead tumor cell (D), on host normal tissue. The flowchart of the simulation procedure is shown in Fig. 5.4. A simulation is terminated after 1000 individual simulations with determined timesteps. A random number (a), in the series of random generating numbers has the value in the range of 0 < a < 1. We distinguish the total tumor cells to one of two possible states:

- (1) proliferating state (i.e. cancer or proliferating tumor cells, P), and
- (2) non-proliferating state or stationary state (i.e. C and D).

For each simulated tumor colony the tumor progress is simulated by the following algorithm:

- (I) At t=0: Initial configuration is five cancer cells in the center of the normal tissue as shown in Fig 5.2 (b).
- (II) At each time step: The rules of cellular automaton are applied to each tumorous cell one by one sequentially selected at random with the same probability and carry out one of the actions upon its state as shown in schematic diagram (Fig. 5.3), described as follows:
- (1) Proliferating state: If the selected cell is the cancer cell, the cancer cell takes one of the following three actions with the function r'_{prolif} and parameter $r_{binding}$.
- (i) The cancer cell may invade the normal cell with the probability r'_{prolif} if this cancer cell has at least one nearest neighbor normal cell (as shown in Fig. 5.2 (a)) randomly chosen with the same probability.
- (ii) The cancer cell is bound by the TICLs with probability $r_{binding}$.
- (iii) The cancer cell may not change with probability $1 (r'_{prolif} + r_{binding})$ or there is no nearest neighboring normal site in the case of invasion with probability r'_{prolif} .
- (2) Stationary state: If the selected cell is in the non-proliferating state, which consists of dead cancer cells and TICLs –tumor complexes that maybe defined as cell complexes.
- (2.1) The complexes: If the selected cell is a complex. The cell may take one of the following three actions with parameters r_{detach} , $r_{binding}$ and r_{lysis} .
- (i) The complexes revert into cancer cells with probability r_{detach} .
- (ii) The complexes may go thru lysis and become dead cancer cells with the probability r_{lysis} .

- (iii) The complexes may not change state with the probability $1 (r_{detach} + r_{lysis})$.
- (2.2) The dead cancer cells: If the selected cell is a dead cancer cell, it takes one of two actions.
- (i) The dead tumor cell may dilute into normal cell with probability r_{decay} .
- (ii) The dead tumor cell may not change with probability $1 r_{decay}$.
- (III) Step (II) continues until the set number of timesteps is reached.

Remark: By this methodology we have to satisfy $r_{prolif.} + r_{binding.} \le 1$ and $r_{detach.} + r_{lysis.} \le 1$.

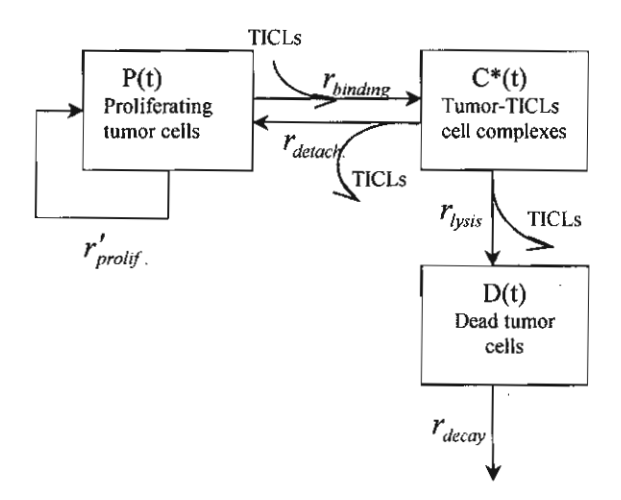


Fig. 5.3 Schematic diagram of cellular automaton model of tumor growth reveals the possible actions, reactions and changing states of each type of tumor cells.

Initial Configuration (t=0): with five proliferating tumor cells in the middle of the tissue model

Setting parameters

: $r_{prolif.}$, $r_{binding}$, $r_{inavt.}$, r_{lysis} , $r_{decay.}$ and K

Setting variables

: n, p, c, d with n(t) = p(t)+c(t)+d(t)

Setting function

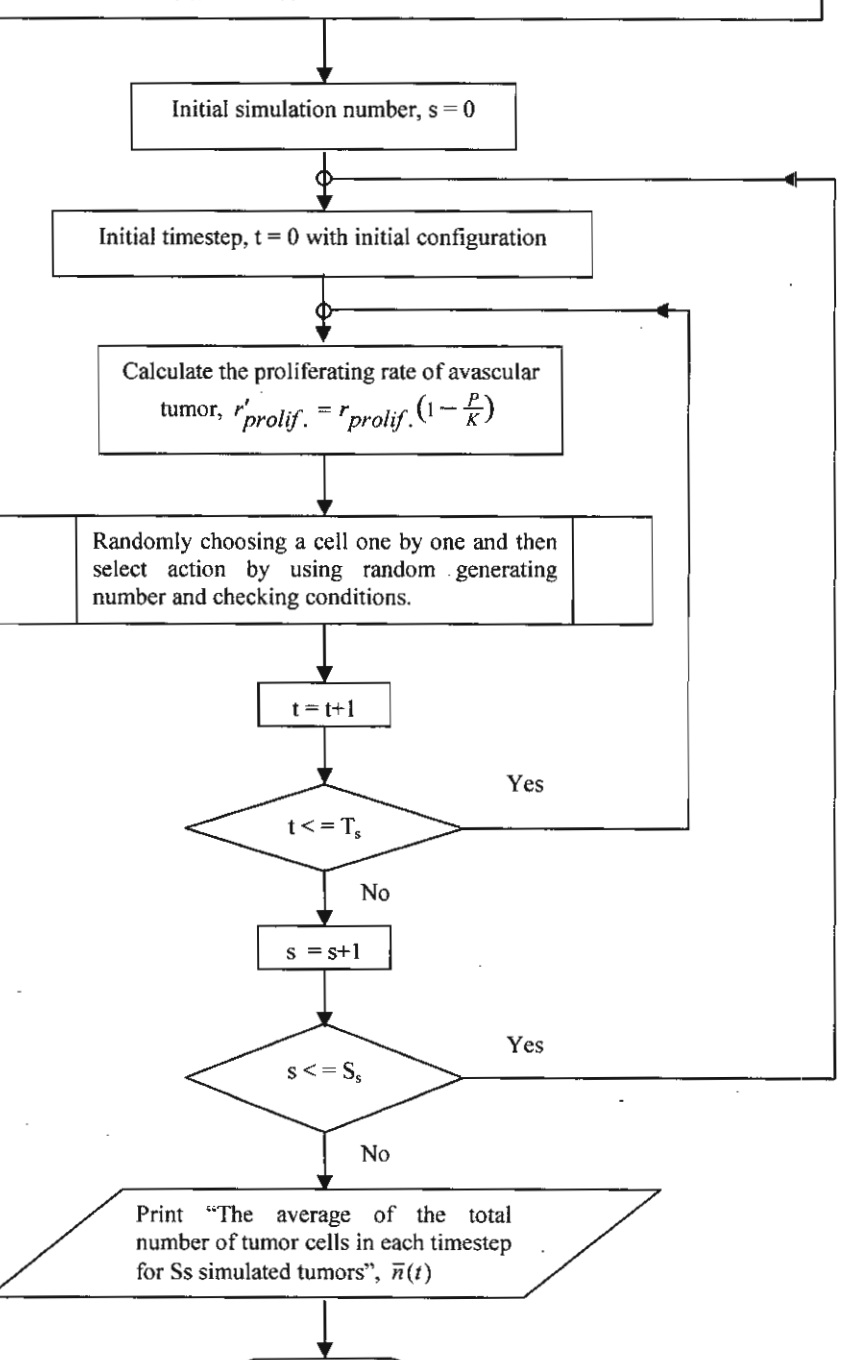
 $: r'_{prolif}$

Setting timestep

: t from 0 to Ts

Setting simulation

: s from 1 to Ss



End

5.1.3 Simulation Results

The methodology described in Section 2 has been transformed into a computer simulation programming. Computer simulation experiments and computational representation of the results in a two-dimensional spatial visualization of tumor invasion of normal tissues are shown in Figures 5.5 (a), 5.5 (b), 55. (f), and 5.5 (g). We denote by P(t) the number of proliferating tumor cells at time t, $C^*(t)$ the number of TICL-tumor cells complexes at time t, and D(t) the number of dead tumor cells at time t. To investigate the evolution of tumor growth, we also denote the total number of tumor cells by $N(t) = P(t) + C^*(t) + D(t)$ Clearly, N(t) can indicate the size of the tumor at time t.

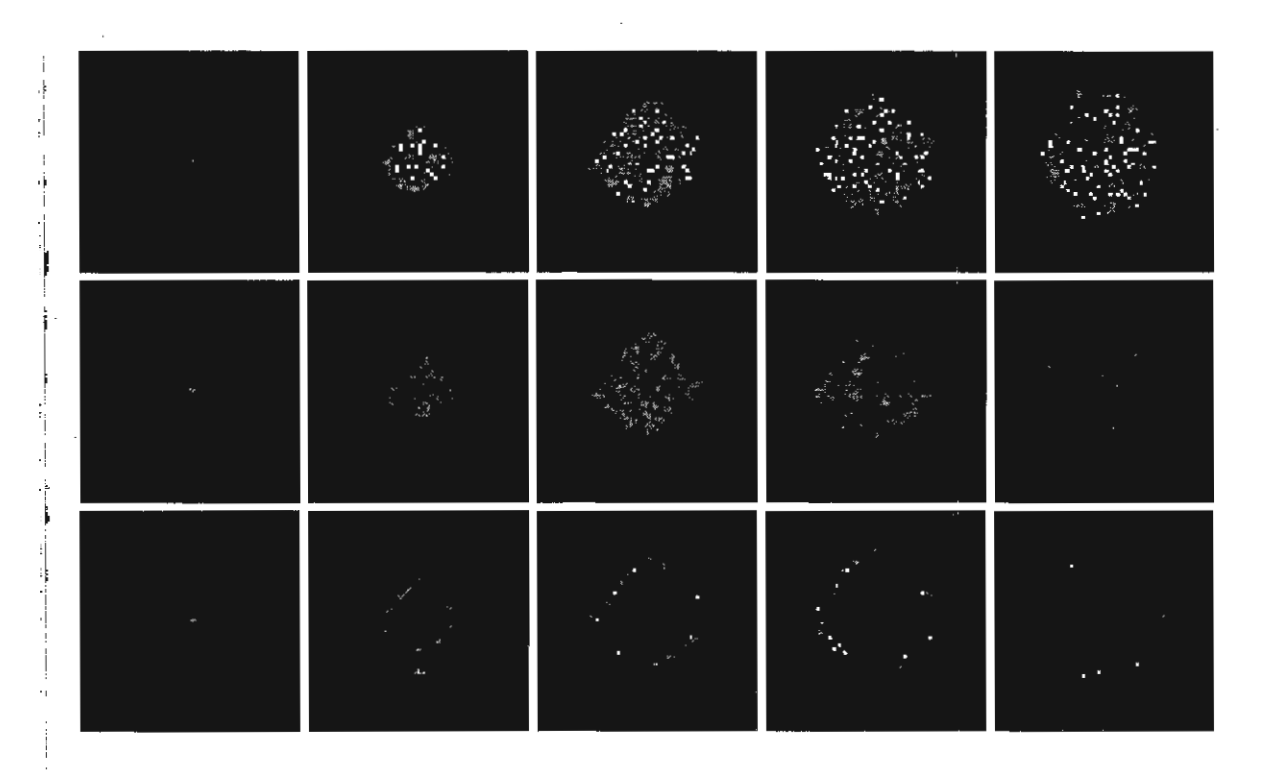


Fig. 5.5 (a) Snapshots of the simulated tumor 61x 61 squared lattice, proliferating cell cluster, and its boundary colony at timesteps 0,15,30,50, and 80. The simulation setting is $r_{prolif.} = 0.85, r_{binding} = 0.1, r_{det ach.} = 0.5, r_{lysis} = 0.35, r_{decay} = 0.35$ and K = 550. Exproliferating tumor cells, : TICLs-tumor cell complexes, Expression dead tumor cells, and Expression cells.

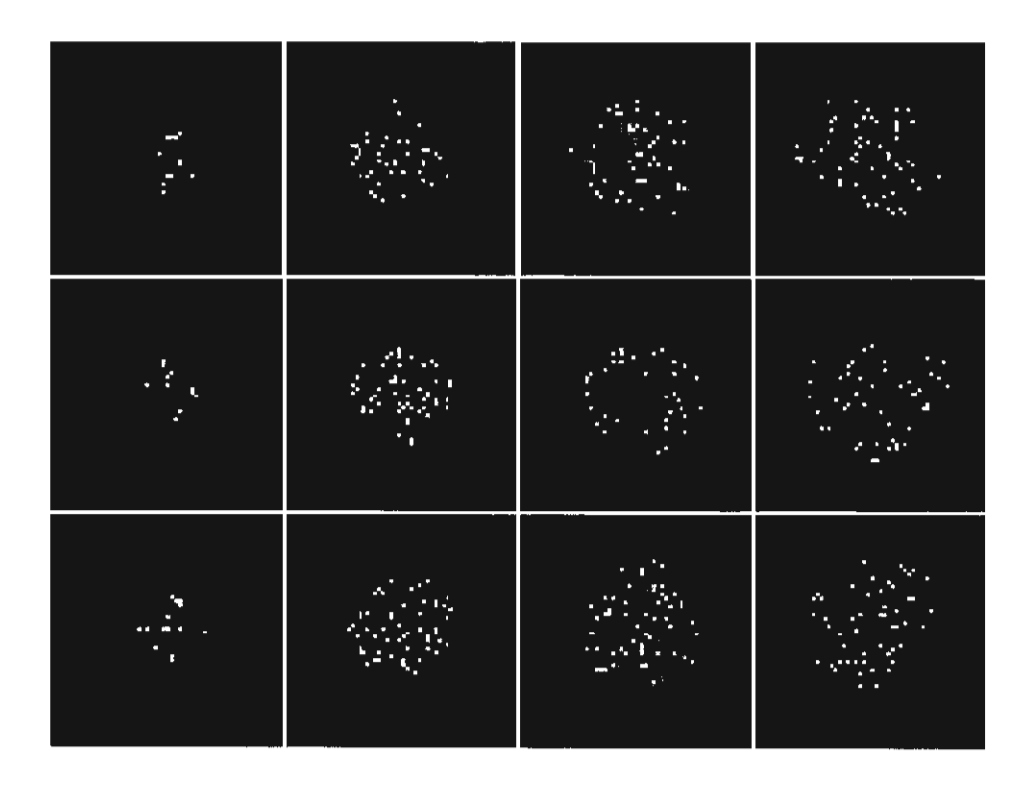


Fig. 5.5 (b) Snapshots of the typical configuration of simulated tumor colonies (61x 61 squared lattice) with the different generating random number and the same simulation setting at timesteps 15, 30, 50, and 80. The simulation setting is $r_{prolif.} = 0.85, r_{binding} = 0.1, r_{detach.} = 0.5, r_{lysis} = 0.35 r_{decay} = 0.35$ and K = 550. \blacksquare : proliferating tumor cells, : TICLs-tumor cell complexes, \blacksquare : dead tumor cells, and \blacksquare : normal cells.

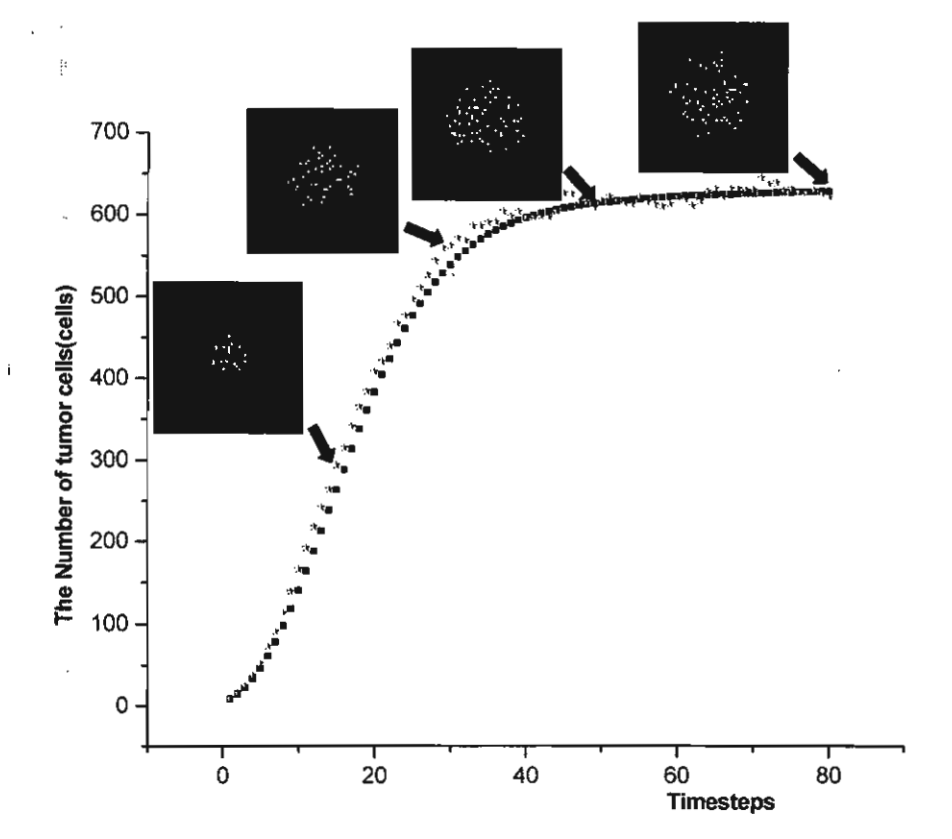
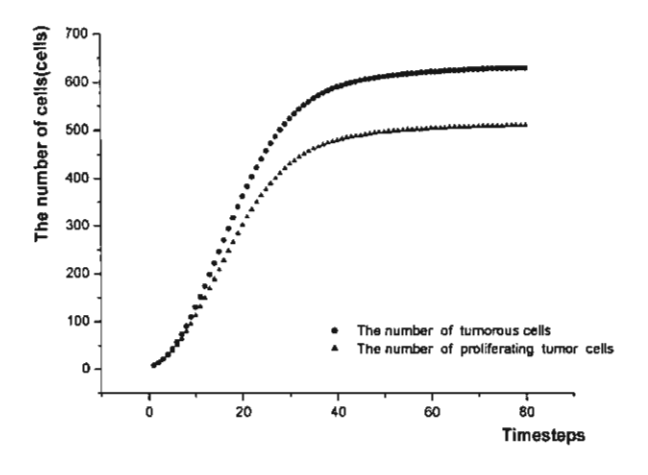


Fig. 5.5 (c) Plots of the time evolutions of the number of cancerous cells dual show with the qualitative shape of simulated multicell tumor. The simulation results are shown for one simulation (star)and averaging over 1000 individual simulations (square), at timesteps 0, 15, 30, 50, and 80. The simulation setting is $r_{prolif.} = 0.85$, $r_{binding} = 0.1$, $r_{detach} = 0.5$, $r_{lysis} = 0.35$, $r_{decay} = 0.35$ and K = 550.



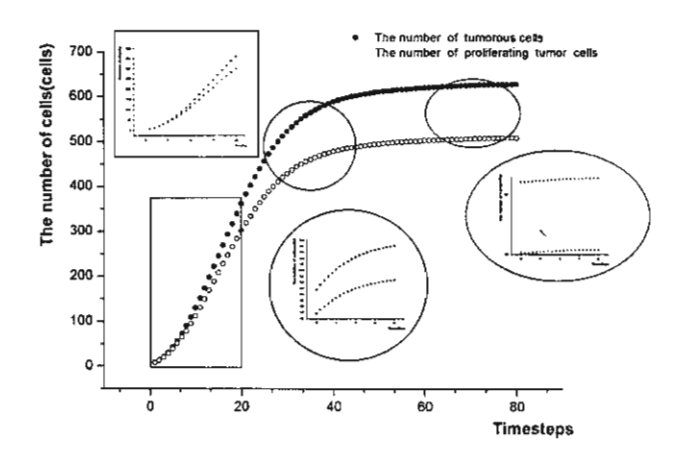


Fig. 5.5 (d) Plots of the time evolutions of the number of tumoral cells (solid circle) and proliferating tumor cells (hollow circle). A part of the curve in typical different figures shows different dynamic growth. The simulational results are the average of 1000 individual simulations, with $r_{prolif.} = 0.85$,

 $r_{binding} = 0.1, r_{det\,ach.} = 0.5, r_{lysis} = 0.35, r_{decay} = 0.35$ and K = 550.

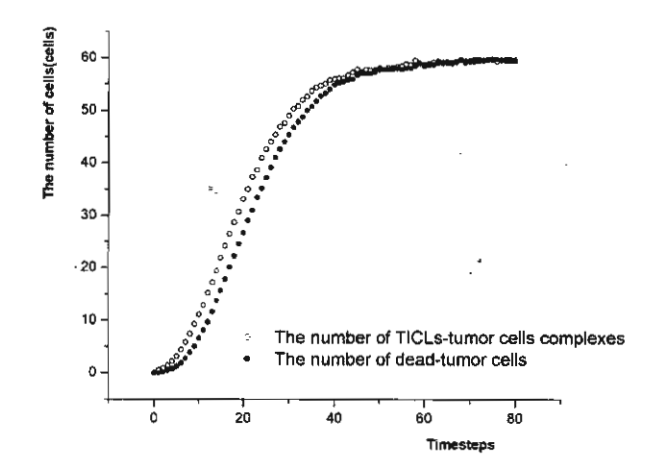


Fig. 5.5 (e) the time evolutions of the number of TICLs-tumor cells complexes (circle) and dead tumor cells (solid circle). The simulational results are the average of 1000 individual simulations, with $r_{prolif.} = 0.85, r_{binding} = 0.1, r_{detach.} = 0.5, r_{lysis} = 0.35, r_{decay} = 0.35$ and K = 550.

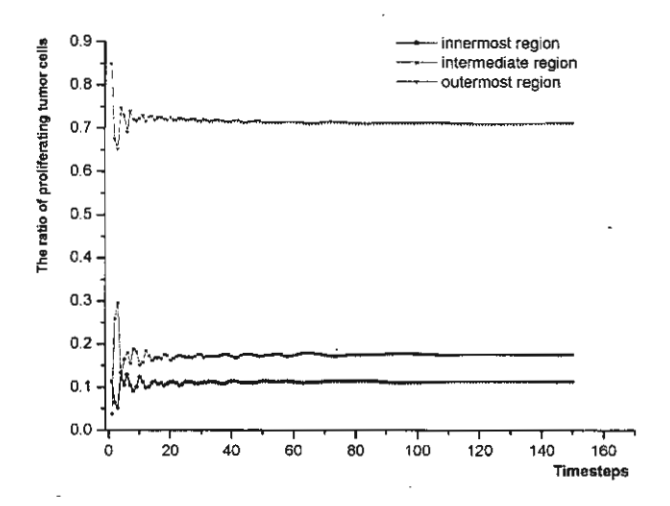


Fig. 5.5 (f) Plots of the ratio of proliferating tumor cell in each region, the innermost, the intermediate and outermost region. The simulation results are the average of 1000 individual simulations, with $r_{prolif.} = 0.85, r_{binding} = 0.1, r_{detach.} = 0.5, r_{lysis} = 0.35, r_{decay} = 0.35$ and K = 550.

1

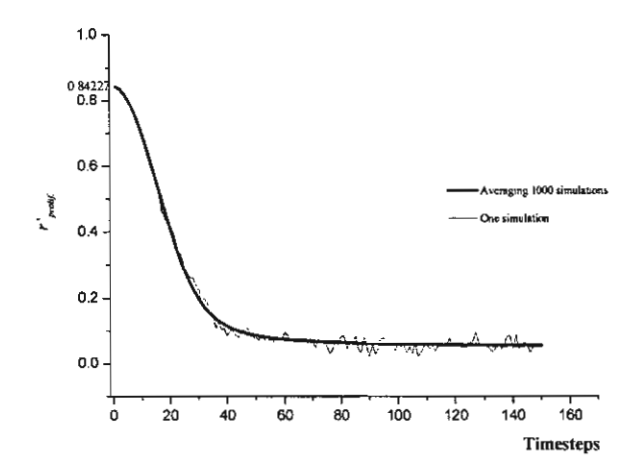


Fig. 5.5 (g) The proliferating function value of avascular tumor growth, r'_{prolif} versus time. The function is defined by $r'_{prolif} = r_{prolif} (1 - \frac{p}{K})$. The average of 1000 individual values of r'_{prolif} from simulated tumor growth (the black solid line) and a typical simulation (gray) have been obtained with $r_{prolif} = 0.85$, $r_{binding} = 0.1$, $r_{detach} = 0.5$, $r_{lysis} = 0.35$, $r_{decay} = 0.35$ and K = 550.

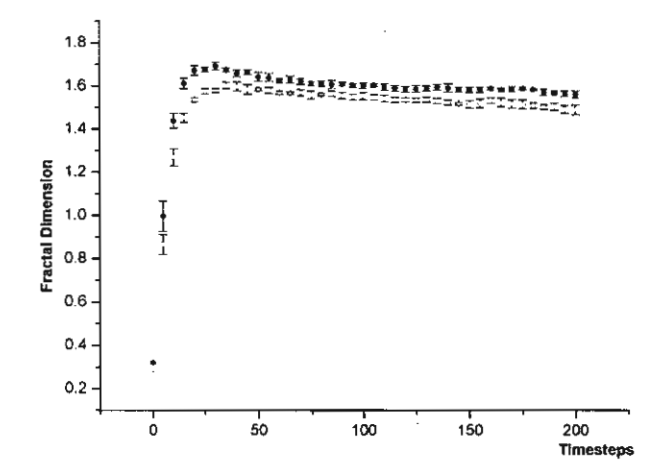


Fig. 5.5 (h) The evolution of fractal dimension of expanding tumor colony (solid circle) proliferating tumor colony by box counting method, using 5 individual colonies. The parameter setting of the five tumor colonies is $r_{prolif.} = 0.85, r_{binding} = 0.1, r_{detach} = 0.5, r_{lysis} = 0.35, r_{decay} = 0.35$ and K = 550.

By the methodology of Cellular automaton model, starting the simulation by placing five proliferating tumor cells in the center of the square lattice, then both later invade and change their states by a series of random generating number to govern the simulated tumor pattern as shown a typical snapshot in different timesteps in Fig. 5.5 (a). Fig. 5.5 (b) reveals a number of simulated colonis made by the different seeds caused by different series of random generating number. Apparently, the morphology of different simulated tumor patterns are different. The growth curve of a typical simulated colony (red star) and the average of 1000 colonies are shown in Fig. 5.5 (c).

The Gompertz growth curve is the best known model, which is successfully used to characterize the experimental data of tumor growth *in vivo* [1, 16, 17], and can be written as

$$V(t) = V_0 \exp\left(\frac{A}{B}(1 - \exp(-Bt))\right), \tag{5.1}$$

where V(t) is the size of tumor at time t, V_0 is the initial volume, while the positive parameters A and B are evaluated by the method of least squares. Based on the CA's model which is described in Section 2.2, the averaged growth curve, as shown in Fig. 5.5 (a) can be described mathematically by Gompertz function approach to Enrich carcinoma mouse growth *in vivo* [17] with the coefficient of nonlinear regression $r^2 = 0.9997$ by computational simulation setting $r_{prolif.} = 0.85$, $r_{binding} = 0.1$, $r_{det ach.} = 0.5$, $r_{lysis} = 0.35$, $r_{decay} = 0.35$, and K=550, and Gompertz parameter setting $V_0 = 2.26 \times 10^{-2} \text{ (cm)}^3$, $A = 0.456 \text{ (days}^{-1})$, $B = 0.102 \text{ (days}^{-1})$. Ultimately, we normalized the data with $V_{max} = 1.94 \text{ (cm)}^3$, and $N_0 = 8.394$, $N_{max} = 625$, as shown in both growth curves in Fig. 5.6. By the growth curves of Fig. 5.6 and the typical five colonies, cell-doubling time versus number of total tumor cells were plotted as shown in Fig. 5.7 with linear relationship.

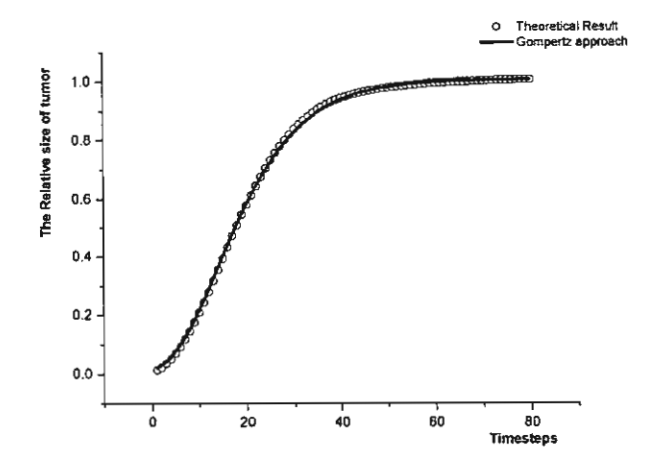


Fig. 5.6 The comparison between the theoretial prediction and the Gompertz approach for the mouse carcinoma Ehrlich with the coefficient of nonlinear regression $r^2 = 0.9997$. Gompertz parameters: $V_0 = 2.26 \times 10^{-2} \, (\text{cm})^3$, $A = 0.456 \, (\text{day})^{-1}$, $B = 0.102 \, (\text{day})^{-1}$ and $V_{max} = 1.94 \, (\text{cm})^3$. The parameters of the model are: with $N_0 = 8.381$, $N_{max} = 627.379$, $r_{prolif.} = 0.85$, $r_{binding} = 0.1$, $r_{detach} = 0.5$, $r_{lysis} = 0.35$, $r_{decay} = 0.35$ and K = 550.

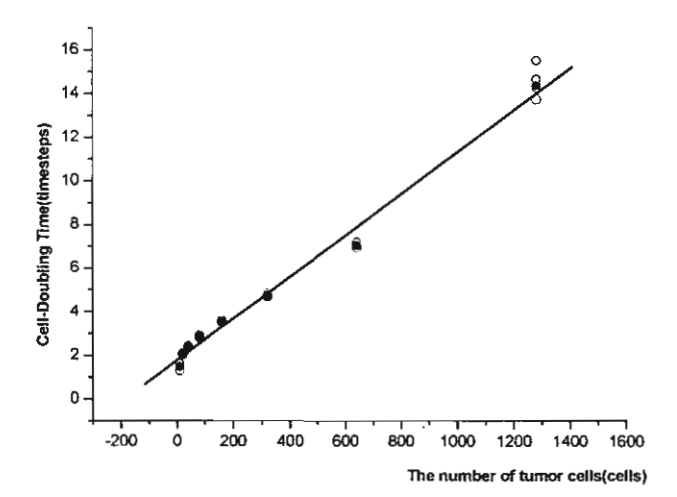


Fig. 5.7 Cells-doubling time versus the number of tumor cells from 1000 individual simulated tumor (solid circle) with five typical individual simulated colonies. The plot of the cell-doubling time of tumor cell number against the number of tumor cells in each colony shows their linear relationship, when parameter setting $r_{prolif.} = 0.85, r_{binding} = 0.1, r_{det\,ach} = 0.5, r_{lysis} = 0.35, r_{decay} = 0.35$ and K = 2000.

The Gompertz curve can be mathematically divided into three regimes as done in [17, 20]. The first regime or early phase, reflects the dynamics of the initial stages of tumorigenesis until the number of tumor cells reaches the value equal to 0.37 of their maximum number of tumor cells within referring time step, which is the time at the infection point on the curve and is defined by t_1 . The second regime, or intermediate phase, of the growth curve is the curve from the first segment, the curve being concave downward until number of tumor cells at crossover time is reached, and the third regime, or saturated phase, begins at the crossover time and lasts until saturated state is reached as seen in Fig. 5.8. In other words, the Gompertzain growth curve can be divided into three regimes by the time at infection point and the crossover time.

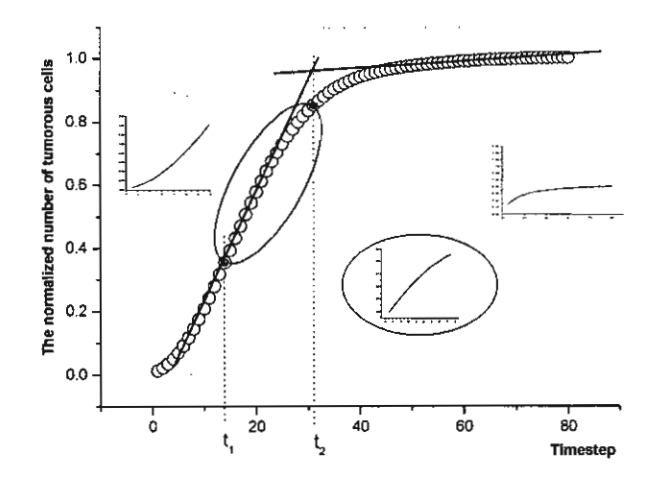


Fig. 5.8 The three segments of sigmoidal Gompertzian curve from simulation result of Fig. 5.4. The first segment has the range from 0 to 14 timesteps within the first solid circle; the second phase covers days 15 until 31; the third phase begins at 32 days beyond the second solid circle.

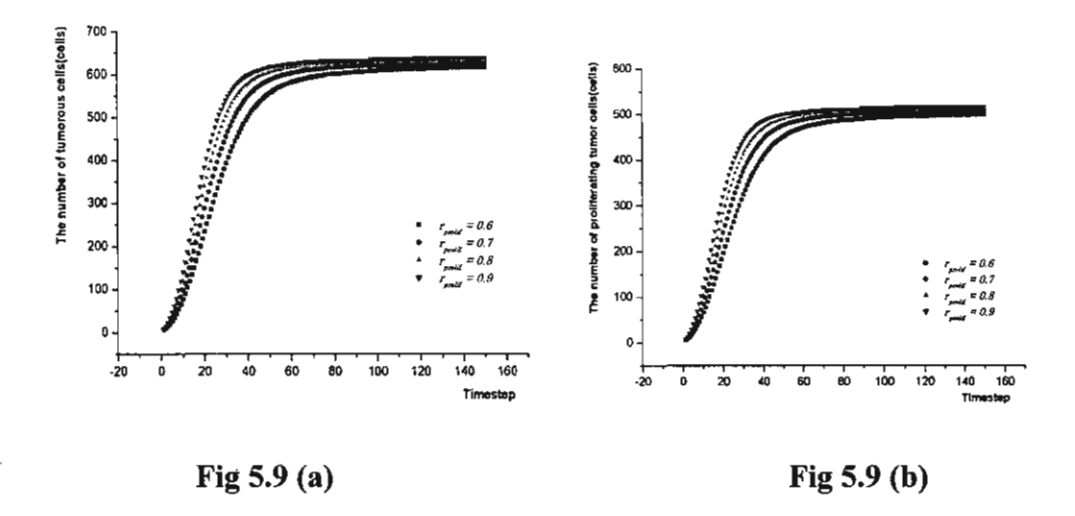
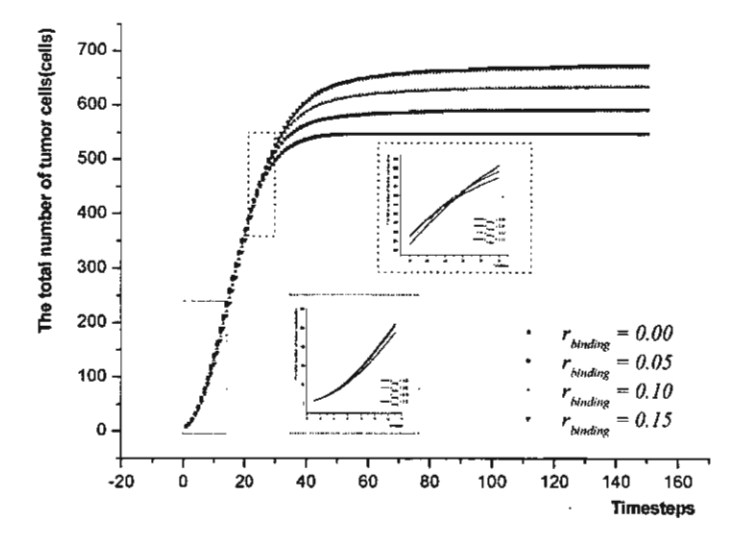


Fig. 5.9 (a) and (b) Plots of the time evolutions of the number of tumoral cells and proliferating tumor cells, respectively. The simulation results are the average of 1000 individual simulations, with parameter $r_{prolif.}$ varying from 0.6 to 0.9 in steps of 0.1, and fixed parameters $r_{binding} = 0.1$, $r_{detach} = 0.5$, $r_{lysis} = 0.35$, $r_{decay} = 0.35$ and K = 550.

Fig. 5.9 shows the simulation results when only r_{prolif} was varied from 0.6 to 0.9 in steps of 0.1, whereas the other parameters were fixed. Fig. 5.9 (a) shows the growth curve of the tumor with varying proliferating rate. We found that the growth rate and saturated tumor cell number are increased with increasing proliferating rate. With the recent finding of crossover time process, the growth curves of a greater proliferating rate will take the shorter crossover time together with the increase in saturated tumor size. By Fig. 5.9 (b), we also reach the same conclusion on the growth curve of total tumor cells as that from Fig. 5.9 (a).



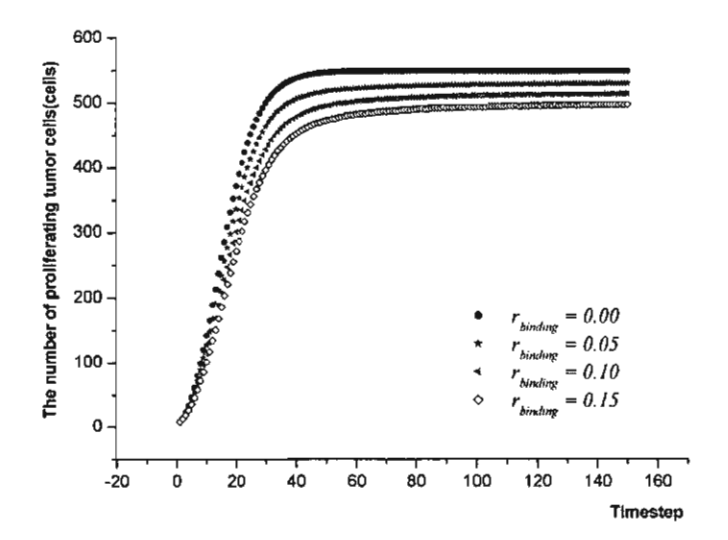
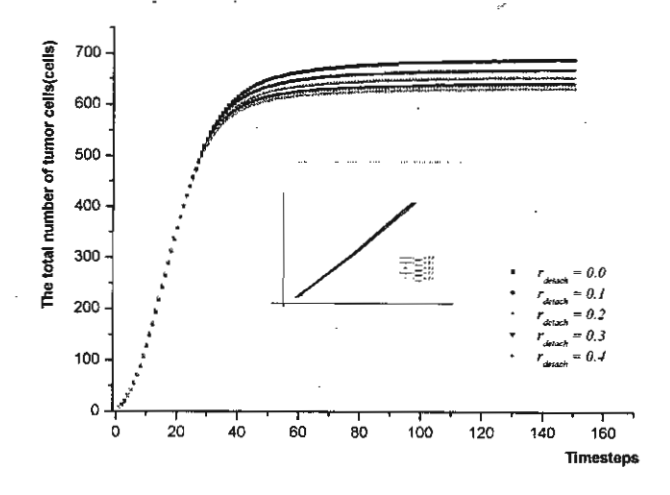


Fig. 5.10 (a) and (b) Plots of the time evolutions of the total number of tumor cells and the number of proliferating tumor cells. The simulation results are the average of 1000 individual simulations, with varying parameter $r_{binding}$, and fixed parameters $r_{prolif.} = 0.85, r_{det\,ach} = 0.5, \ r_{lysis} = 0.35, \ \text{and} \ K = 550$.

In order to investigate the role of immune system within this model which is represented by the values of the parameters $r_{binding}$ and, r_{detach} . We consider the growth curve of tumor when only $r_{binding}$ is varied, with other parameters fixed as illustrated in Fig. 5.10 (a), while the growth curve of tumor with varying r_{detach} and other parameters fixed is shown in Fig. 5.11 (a). Certainly, increasing the binding rate of TICLs, will increase the binding rate effect in delaying or inhibiting tumor proliferation. Figures 5.10 (a) and (b) show that when $r_{binding}$ is increased, the growth curve will have more crossover time, which means that the system will take more time to reach the saturated phase. In more detail, considering the first regime of the growth curves in Fig. 5.10 (a) (t = 1 to 13), the growth will decrease with increasing $r_{binding}$, which shows that the first regime is effected by the number of proliferating cells more than other cell types. Between timesteps 25 and 29, each growth curve flips until the growth increases with increasing $r_{binding}$, and the third regime is reached with higher saturated size of tumor for higher value of $r_{binding}$. Apparently, according to Fig. 5.10 (b), the growth of proliferating cells decreases and the saturated number of proliferating cell decreases with increasing $r_{binding}$, since the binding role of immune system is to decrease the number of proliferating tumor cells. According to Figures 5.10 (a) and (b), varying the parameter $r_{binding}$ indicates that higher number of proliferating cells does not necessary mean larger tumor size. Moreover, $r_{binding} = 0.0$ refers to the proliferating tumor cells growing stochastically on two-dimensional square lattice with von Neuman neighborhood.



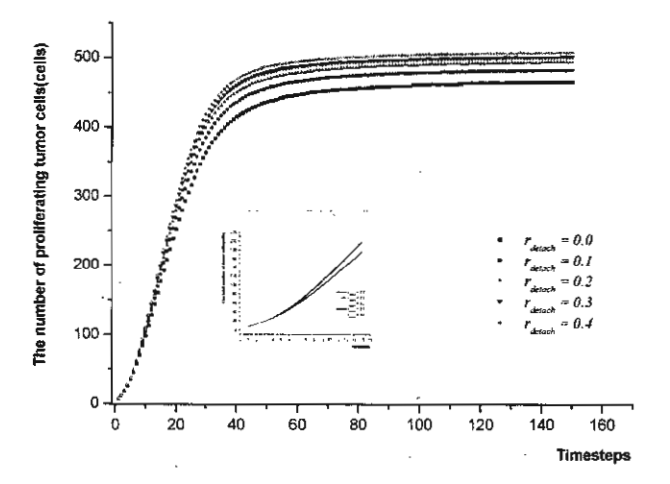


Fig. 5.11 (a) and (b) Plots of the time evolutions of the total number and the number of proliferating tumor cells of simulated tumor. The simulation results are the average of 1000 individual simulations with r_{detach} , varying from 0.0 to 0.4 in steps of 0.1, and fixed parameters $r_{prolif.} = 0.85$, $r_{binding} = 0.1$, $r_{lysis} = 0.35$, $r_{decay} = 0.35$ and K = 550.

To investigate the influence of the r_{detach} , we fixed the other parameters and vary this rate from 0.0 to 0.4 in steps of 0.1. According to Fig. 5.11 (a), we found that increasing r_{detach} will decrease the crossover time of the growth curve, which means that the system will use shorter time to reach the saturated regime. However, the saturated size of the tumor will decrease with lower r_{detach} . Considering Fig. 5.11 (b), increasing r_{detach} will lead to an increase in the number of proliferating tumor cell, larger saturated tumor size and less crossover time.

investigating the morphology of simulated tumor colony. Clinically, Bru et al. [27] have defined the three regions of avascular tumor via the radius of tumor (R), namely, an innermost region $(0 \le r_i < \frac{R}{2})$, an intermediate region $(\frac{R}{2} \le r_i < \frac{4R}{5})$, and an outermost region $r_i \ge \frac{4R}{5}$, where r_i is the radius of tumor colony from the origin. They measured the proliferating cell of human colon adenocarcinoma colony in each region, the innermost region covers 6% of proliferating cells and 25% of the whole colony surface, the intermediate region covers 14% of proliferating cells and 39% of the whole colony surface, and the outermost region consists of 80% of proliferating cells and 36% of the whole colony surface. We also measured this quantity by computational algorithm applied to each simulated tumor colony and we also found that the averaging ratio of proliferating cell in the outtermost region is greater than those of both other regions by 70%, 18% and 12% respectively as shown in Fig. 5.5 (f). The simulation results indicated that proliferating cells are located mainly to the outtermost region which corresponds to the experimental data *in vivo* of Bru et al [27].

We have been interested in the qualitative result of avascular tumor growth model,

It is found that the colonies obtained from the stochastic model have an approximately circular shape with a rough boundary as shown in Figures 5.5 (a) and (b). A few researchers [6, 7, 8, 22, 23, 25, 26] were interested in the fractal dimension of the stochastic growth model. We defined the boundary cells of the simulated tumor growth by assuming that the boundary cells are the outtermost cells covering the colony in each row and each column in the lattice. We also found the fractal dimension of the expansion of multicell tumor colony and the proliferating tumor cell against timesteps using Beniot 1.3 [36] as shown in Fig. 5.5 (h).

At each time step, if we let S be the number of tumor cells on the tumour periphery. The center of mass of the boundary with coordinates (x_n, y_n) is defined as

$$(\overline{x}, \overline{y}) = \frac{1}{S} \sum_{\text{periphery}} (x_n, y_n)$$
 (5.2)

The mean radius of the boundary is defined as

$$R = \frac{1}{S} \sum_{\text{periphery}} \sqrt{\left(x_{n} - \overline{x}\right)^{2} + \left(y_{n} - \overline{y}\right)^{2}}$$
 (5.3)

A

The squared mean thickness of the boundary is defined as

$$\sigma^{2} = \frac{1}{S} \sum_{\text{periphery}} \left[\sqrt{\left(x_{n} - \overline{x}\right)^{2} + \left(y_{n} - \overline{y}\right)^{2}} - R \right]^{2}$$
 (5.4)

For each colony, using least square method to find α and β in the relation

$$\sigma = \alpha R^{\beta} \tag{5.5}$$

By equation (5.5), the value of β indicates how the dynamics of boundary growth depends on the power law. We used the individuals of 1000 colonies for each timestep through to 35 timesteps, from the simulated result in Fig. 5.5, then we obtained $\alpha = 0.23439 \pm 0.01456$, and $\beta = 0.63339 \pm 0.02581$ with $r^2 = 0.96746$. Our results are different from the result given in [23] and [26], the stochastic cluster growth on a plane, which found that $\beta = 0.468 \pm 0.092$.

However, we obtained the same conclusion on the fractality of the boundary. Thus, we can conclude from the fractional value of β that the boundary is fractal. Which means that it has the same amount of roughness when enlarged [23]. By the equation (5.5), Wang et al. [26] concluded that if β < 1, the larger colonies have smaller relative boundary thickness.

In conclusion, the CA model showed that the macroscopic behavior of a tumor can be affected by setting the presence of an immune system response at microscopic scale. In addition, the analysis of the morphology of simulated patterns by scaling law and the growth rate of tumor in each phase of the Gompertzian curve were presented.

The cellular automata model on a three-dimensional square lattice with simulation results is in progress.

Other related activities

Apart from the work explained above on what has been proposed in this project, we have spent some of our time in investigating different techniques of modelling and simulation of cell division in various aspects. This part of our work has resulted in 3 published papers as can be seen in Appendices # 5.1-5.3. The work on growth of Leptospire (in Appendix # 5.1) is done in support of the research work in Subproject 3, while the work on bacteria cell division (Appendix # 5.3) will be of great use to the continued research on bacterial growth and drug resistance in Subproject 1.

Table V: Proposed and Actual Activity for Subproject 5.

| Months | Month | Months | Months | Months | Months |
|-----------------------|-----------------------|------------|-------------------|-----------------------|----------------------------|
| 1-6 | 7-12 | 13-18 | 19-24 | 25-30 | 31-36 |
| <> | | | | | |
| \longleftrightarrow | | ļ | | | |
| | | | | | |
| | \longleftrightarrow | | | | |
| | | | | | |
| | | | | İ | |
| | ← | | | | |
| | | : | | | |
| | | ~ | | | |
| | | · | \longrightarrow | : | |
| | | | | | |
| | | | | | |
| | | | | <u></u> | |
| | | | | \longleftrightarrow | |
| | | | | | |
| | | | | _ | |
| | | | | <u> </u> | |
| | | | | | |
| | | j | | * | |
| | | | | ` | |
| | | | | | |
| | | · | | | |
| | | | | | |
| | | | | | |
| | | | | | |
| | 1-6 | 1-6 7-12 < | 1-6 7-12 13-18 < | 1-6 7-12 13-18 19-24 | 1-6 7-12 13-18 19-24 25-30 |

^{*} The investigator has become interested in investigation of different simulation techniques for other cell divisions instead.

Outputs of Subproject 5

Papers appeared/accepted in international journals 3

Paper presented in international conference

1

Subproject 6: Research on Asymptotic Stability of Difference Equations with Delays

Principal Investigator: Dr. Piyapong Niamsup

The research work in this subproject may be summarized year by year as follows.

6.1 Year 1:

During the first year, we mainly studied the asymptotic stability of linear difference equations of the form

$$x_{n+1} - a^2 x_{n-1} + b x_{n-k} = 0 ag{6.1}$$

where a and b are arbitrary real numbers, k is a positive integer and n = 0,1,2,... The motivation for studying the above difference equations came from a paper of S.A. Kuruklis [1] in which he gave the necessary and sufficient conditions for asymptotic stability for the linear difference equation of the form

$$x_{n+1} - ax_n + bx_{n-k} = 0 ag{6.2}$$

where a and b are arbitrary real numbers, k is a positive integer and n = 0,1,2,... The main result in [1] reads as follows:

Theorem A Let a be a nonzero real, b an arbitrary real, and k a positive integer greater than 1. Equation (6.2) is asymptotically stable if and only if $|a| < \frac{k+1}{k}$, and

$$|a|-1 < b < {a^2 - 2|a|\cos\phi + 1}^{\frac{1}{2}}$$
 for k odd
 $|b-a| < 1$ and $|b| < {a^2 - 2|a|\cos\phi + 1}^{\frac{1}{2}}$ for k even

where ϕ is the solution in $\left(0, \frac{\pi}{k+1}\right)$ of $\frac{\sin k\theta}{\sin(k+1)\theta} = \frac{1}{|a|}$.

Our main result on asymptotic stability of equation (6.1) is obtained as follows:

Theorem 1 Let a be a nonzero real, b an arbitrary real, and k a positive integer greater than

1. Equation (6.1) is asymptotically stable if and only if

$$|a| < 1$$
 and $a^2 + |b| < 1$ for k even
$$|a| < \sqrt{\frac{k+1}{k-1}} \text{ and } a^2 - 1 < b < \{a^4 - 2a^2 \cos 2\phi + 1\}^{\frac{1}{2}} \text{ for k odd}$$

where ϕ is the solution in $\left(0, \frac{\pi}{k+1}\right)$ of $\frac{\sin(k-1)\theta}{\sin(k+1)\theta} = \frac{1}{a^2}$.

Remark 1. Note that when a = 0 or k = 1 it is easy to show that the necessary and sufficient conditions for (6.1) to be asymptotically stable is that $|a^2 - 1| < 1$.

2. The technique of proof in a main step of Theorem 1 is somewhat different from that in Theorem A so that we pointed out an error of the proof of Theorem A in [1].

References

[1] S.A. Kuruklis, The Asymptotic Stability of $x_{n+1} - ax_n + bx_{n-k} = 0$, J. Math. Anal. Appl. 188 (1994), 719-731.

6.2 Year 2:

Continuing from the first year, in the beginning of the second year we have investigated the necessary and sufficient conditions for asymptotic stability of the following linear delayed difference equation:

$$X_{n+1} - X_{n-1} + p \sum_{i=1}^{N} X_{n-k+(j-i)l} = 0$$
 (6.3)

where n is a nonnegative integer, p is a real number, k, l and N are positive integers where k > (N-1)1. The idea of this investigation began when we read through a paper written by R. Ogita, H. Matsunaga, and T. Hara [1], where they gave the necessary and sufficient conditions for the asymptotic stability of the following linear delayed difference equation

$$x_{n+1} - x_n + p \sum_{i=1}^{N} x_{n-k+(j-1)i} = 0$$
 (6.4)

where n is a nonnegative integer, p is a real number, k, l and N are positive integers where k > (N-1)1. The following is the main result obtained in [1]:

Theorem 1 Let k, l and N be positive integers with k > (N-1)1. Then the zero solution of (6.4) is asymptotically stable if and only if

$$0$$

where M = 2k + 1 - (N-1)1.

Using similar technique as in [4] we are able to obtain the necessary and sufficient conditions for the asymptotic stability of (3) as follows:

Theorem 2 Let k, l and N be positive integers with k odd, l even and k > (N-1)1. Then the zero solution of (6.4) is asymptotically stable if and only if

$$0$$

where M = 2k - (N-1)1.

<u>Theorem 3</u> Let k, l and N be positive integers with k and l odd and k > (N-1)l. Then the zero solution of (6.4) is asymptotically stable if and only if

$$0$$

where
$$M = 2k - (N-1)l$$
, $p_0^* = min\{p_0, p^*\}$, $p_0 = \frac{2sin\left(\frac{\pi}{M}\right)sin\left(\frac{l\pi}{2M}\right)}{sin\left(\frac{Nl\pi}{2M}\right)}$,

$$p' = \min \left\{ p_m : m = \left[\frac{M}{4} - \frac{1}{2} \right] + 1, \left[\frac{M}{4} - \frac{1}{2} \right] + 2, \dots, \frac{M}{2} - 1 \right\},$$

$$p_{m} = 2(-1)^{m+1} \frac{\sin w_{m} \sin \frac{lw_{m}}{2}}{\sin \frac{Nlw_{m}}{2}} \text{ and } w_{m} = \frac{2m+1}{M}\pi.$$

We note that the main tool in the proof is the analysis of the locations of the roots of the characteristic equation of (6.3) to obtain the criterion for these roots to be located inside the unit disk which imply the asymptotic stability of the zero solution of (6.3).

Similarly, we have the following result:

<u>Theorem 4</u> Let k, l and N be positive integers with $k \ge (N-1)1$. Then the zero solution of

$$X_{n+1} + p \sum_{i=1}^{N} X_{n-k+(i-1)1} = 0$$
 (6.5)

is asymptotically stable if and only if

$$-\frac{1}{N}$$

where p_{min} is the smallest positive real value of p for which the characteristic equation of (6.5) has a root on the boundary of the unit circle.

The other topics that we have been studying are the controllability and stability of Chen chaotic dynamical system given by

$$\dot{x} = a(y - x)$$

$$\dot{y} = (c - a)x - xz + cy$$

$$\dot{z} = xy - bz$$
(6.6)

where a, b, c are positive real parameters. In [2], H.N. Agiza and M.T. Yassen studied synchronization of system (6.6) using adaptive control. In [3], Y. Wang, Z.H. Guan and X. Wen studied adaptive synchronization of system (6.6) with fully unknown parameters. In [4], M.T. Yassen studied the optimal control of system (6.6). Motivated by these results we are interested in controllability and stability of the following modified Chen chaotic dynamical system

$$\dot{x} = a(y-x)$$

$$\dot{y} = (c-a)x - xz + cy$$

$$\dot{z} = xy - bz + dx^{2}$$
(6.7)

where a, b, c, d are positive real parameters. We are interested in studying the control of chaos in the system (6.7) using linear feedback controls and bounded feedback controls, the sufficient conditions on parameters which ensure the stabilities of equilibrium points, and the synchronization of system (6.7) using adaptive control and active control.

References

- [1] R. Ogita, H. Matsunaga, and T. Hara, Asymptotic Stability for a Class of Linear Delay Difference Equations of Higher Order, *J. Math. Anal. Appl.* 248 (2000), 83-96.
- [2] H.N. Yagiza and M.T. Yassen, Synchronization of Rossler and Chen Chaotic Dynamical System, *Physic Letter A*, 278 (2001), 191-197.
- [3] Y. Wang, Z.H. Guan and X. Wen, Adaptive Synchronization for Chen Chaotic System with Fully Unknown Parameters, *Chaos Solitons and Fractals*, 19 (2004), 899-903.
- [4] M.T. Yassen, The Optimal Control of Chen Cahotic Dynamical System, Applied Math. Comput., 131 (2002), 171-180.

6.3 Year 3:

In year 3, one of our papers has appeared, namely

1. T. Kaewong, P. Niamsup and Y. Lenbury, A note on asymptotic stability conditions for delay difference equations. *International Journal of Mathematics and Mathematical Sciences*. 7 (2005) 1007-1013.

Note that in this manuscript, we have studied the asymptotic stability of $x_{n+l} + p \sum_{i=1}^{N} x_{n-k+(j-l)i} = 0 \text{ and we obtained the following result:}$

<u>Theorem 1</u> Let k, l and N be positive integers with $k \ge (N-1)1$. Then the zero solution of

$$X_{n+1} + p \sum_{i=1}^{N} X_{n-k+(j-1)1} = 0$$
 (6.8)

is asymptotically stable if and only if

$$-\frac{1}{N}$$

The idea of this investigation began when we read through a paper written by R. Ogita, H. Matsunaga, and T. Hara [1], where they gave the necessary and sufficient conditions for the asymptotic stability of the following linear delayed difference equation

$$x_{n+1} - x_n + p \sum_{i=1}^{N} x_{n-k+(j-1)i} = 0$$
 (6.9)

where n is a nonnegative integer, p is a real number, k, l and N are positive integers where k > (N-1)l. The following is the main result obtained in [1]:

<u>Theorem 2</u> Let k, l and N be positive integers with k > (N-1)1. Then the zero solution of (6.4) is asymptotically stable if and only if

$$0$$

where M = 2k + 1 - (N-1)1.

We have been investigating the following difference equation similar to (6.8) and (6.9):

$$X_{n+1} - \alpha X_n + p \sum_{j=1}^{N} X_{n-k+(j-1)1} = 0$$
 (6.10)

where $0 \le \alpha \le 1$. We note that when $\alpha = 0$, (6.10) becomes (6.8); and when $\alpha = 1$, (6.10) becomes (6.9). Thus, it is natural to study the asymptotic stability of (6.10).

In year 2, we studied the controllability and stability of perturbed Chen chaotic dynamical system given by

$$\dot{x} = a(y-x)$$

$$\dot{y} = (c-a)x - xz + cy$$

$$\dot{z} = xy - bz + dx^{2}$$
(6.11)

where a, b, c, d are positive real parameters.

We continue our work to the perturbed Chua's circuit system given by

$$\dot{x} = p \left(y - \frac{1}{7} (2x^3 - x) \right)$$

$$\dot{y} = x - y + z$$

$$\dot{z} = -qy + rx^2$$
(6.12)

where p, q, r are positive real parameters. We are interested in studying the control of chaos in the system (6.12) using linear feedback controls and bounded feedback controls, the sufficient conditions on parameters which ensure the stabilities of equilibrium points, and the synchronization of the system (6.12) when the parameters of the drive system are fully unknown and different with those of the response system using adaptive control and active control. See [1]-[3] for more details.

References

[1] J.H. Park, Chaos Synchronization between Two Different Chaotic Systems Using Active Control, Chaos, Solitons and Fractals, 2005, in press.

- [2] M.T. Yassen, Adaptive Control and Synchronization of a Modified Chua's Circuit System, *Applied Mathematics and Computation*, 135(2003), 13-128.
- [3] M.T. Yassen, Adaptive Synchronization of Rossler and Lu Systems with Fully Uncertain Parameters, Chaos, Solitons and Fractals, 23(2005), 1527-1536.

Table VI: Proposed and Actual Activity for Subproject 6.

| Activity: Proposed (<->) | Months | Month | Months | Months | Months | Months |
|--------------------------------|-------------|-------------|-----------------|--------|-----------------|--|
| Actual (\longleftrightarrow) | 1-6 | 7-12 | 13-18 | 19-24 | 25-30 | 31-36 |
| 1. Collect papers, books. | <> | | | | | |
| 2. Study techniques used in | | ·> | | | | |
| papers and books. | ← | | | | | |
| 3. Research to obtain new | < | | - | | | |
| results. | | | | | > | |
| 4. Submit papers for | | - | < | | | |
| publications. | | | < | | | |

Outputs of Subproject 6

Papers appeared/accepted in international journals 4

Master graduates 6

7. OVERALL OUTPUT

7.1 Summary table

Ėį.

| Subproject | Appeared/ Accepted | Inter. Conference | Ph.D. graduates | Masters graduates |
|------------|-----------------------|-------------------|--------------------|----------------------|
| 1 | 8 | 2 | 6 | 1 |
| 2 | 1 | 2 | 2 | - |
| 3 | 14 | 3 | 4 | 9 |
| 4 . | - | 3 | - | 3 |
| 5 | 3 | 1 | - | - |
| 6 | 4 | | - | . 6 |
| Total | 30 | 11 | 12 | 19 |

7.2 Rank promotions

4 rank promotions:

Dr. Julian Poulter promoted to Full Professor
 Asst. Prof. Nardtida Tumrasvin promoted to Associate Professor
 A. Somkid Amornsamankul promoted to Assistant Professor
 Dr. Wannapong Triampo promoted to Assistant Professor

7.3 Publications output of the project

Subproject 1

- Dumrongpokaphan, T., Lenbury, Y. Cascade Mechanism in a Selfregulatory Endocrine System: Modelling Pulsatile Hormone Secretion. *Pure* and Applied Chemistry. 74(6) (2002) 881-890.
- Lenbury, Y., Pansuwan, A., Tumrasvin, N. Chaos and Control Action in a Kolmogorov Type Model for Food Webs with Harvesting or Replenishment. Science Asia. 28(3) (2002) 205-215.
- 3. Rattanakul, C., Lenbury, Y., Krishnamara, N., Wollkind, D.J. Modeling of Bone Formation and Resorption Mediated by Parathyroid Hormone: Response to Estrogen/PTH Therapy. *BioSystems*. **70(1)** (2003) 55-72.
- Dumrongpokaphan, T., Lenbury, Y., Crooke, P.S. The Analysis of Higher-Order Cascade Systems with Separation Conditions Pivoting on the Slow Components: Application to a Model of Migration for Survival of the Species. Mathematical and Computer Modelling. 38 (2003) 671-690.
- Lenbury, Y., Giang, D.V. Nonlinear Delay Differential Equations Involving Population Growth. Mathematical and Computer Modelling. 40 (2004) 586-590.
- Lenbury, Y., Pornsaward, P. A Delay-differential Equation Model of the Feedback-controlled Hypothalamus-pituitary-adrenal Axis in Humans. *Mathematical Medicine and Biology: A Journal of the IMA*. 22 (2005) 15-33.
- 7. Crooke, P.S., Kongkul, K., Lenbury, Y., Adams, A.B., Carter, C.S., Marini, J.J., Hotchkiss, J.R. Mathematical Models for Pressure Controlled Ventilation of Oleic Acid-injured Pigs. *Mathematical Medicine and Biology.* **22** (2005) 99-112.

 Giang, D.V., Lenbury, Y., Seidman, T.I. Delay Effect in Models of Population Growth. *Journal of Mathematical Analysis and Applications*. 305 (2005) 631-643.

Subproject 2

4

ä

4

• 1

.

:1

ij

ij,

1

ì

d

ij.

H

 Poltem, D., Wiwatanapataphee, B., Ruengsakulrach, P., Lenbury, Y., Punpocha, M., Wu, Y.H. A Numerical Study of Blood Flow Patterns in Coronary Artery Bypass Grafts. *Quantitative Methods*. 1(1) (2004) 1-7.

Subproject 3

- Pongsumpun, P., Yoksan, S., Tang, I.M. A Comparison of the Age Distributions in the Dengue Hemorrhagic Fever Epidemics in Santiago de Cuba (1997) and Thailand (1998). Southeast Asian Journal of Tropical Medicine and Public Health. 33 (2002) 255.
- Pongsumpun, P., Lenbury, Y., Tang, I.M. Age Structure in a Model for the Transmission of Dengue Hemorrhagic Fever in Thailand. *East-West Journal* of Mathematics. Special Volume (2002) 93-103.
- Kammanee, A., Lenbury, Y., Tang, I.M. Transmission of Plasmodium Vivax Malaria. East-West Journal of Mathematics. Special Volume (2002) 277-284.
- Kanyamee, N., Lenbury, Y., Tang, I.M. The Effect of Migrant Workers on the Transmission of Malaria. East-West Journal of Mathematics. Special Volume (2002) 297-308.
- 5. Pongsumpun, P., Tang, I.M. Transmission of Dengue Hemorrhagic Fever in an Age Structured Population. *Math. Comp. Model.* **37** (2003) 949-961.
- Kaewmanee, C., Tang, I.M. Cannibalism in an Age-structured Predator-prey System. Ecol. Modelling 167 (2003) 213-220.
- Sriprom, M., Pongsumpun, P., Yoksan, S., Barbazan, P., Gonzales, J.P., Tang, I.M. Dengue Haemorrhagic Fever in Thailand 1998-2003: Primary or Secondary. *Dengue Bulletin*. 27 (2003) 39-45.
- 8. Nishiura, H., Tang, I.M., Kakehashi, M. The Impact of Initial Attack Size on Sars Epidemic for SARS Free Countries: Possible Reason for Japan without a Domestic Transmission. *Journal of Medical Safety*. **1(1)** (2003) e1-e6.
- Pongsumpun, P., Patanarapelert, K., Sriprom, M., Varamit, S., Tang, I.M. Infection Risk to Travellers Going to Dengue Fever Regions. Southeast Asian Journal of Tropical Medicine and Public Health. 35 (2004) 155.

- Naowarat, S., Tang, I.M. Effect of Bird-to-bird Transmission of the West Nile Virus on the Dynamics of the Transmission of this Disease. Southeast Asian Journal of Tropical Medicine and Public Health. 35 (2004) 162.
- Nishiura, H., Patanaraspelert, K., Sriprom, M., Sarakorn, W., Sriyab, S., Tang, I.M. Modelling Potential Responses to Severe Acute Respiratory Syndrome (SARS) in Japan: the Role of Initial Attack Size, Precaution and Quarantine. J. Epid. Commun. Health. 58(3) (2004) 156.
- Nishiura, H., Tang, I.M. Modeling for a Smallpox-vaccination Policy against Possible Bio-terrorism in Japan: The Impact of Long-lasting Vaccinal Immunity. J. Epid. 14(2) (2004) 41.
- Nishiura, H., Patanarapelert, K., Khortwong, P., Tang, I.M., Pasakorn, A.
 Predicting the Future Trend of Drug-resistant Tuberculosis in Thailand:
 Assessing the Impact of Control Strategy. Southeast Asian Journal of Tropical Medicine and Public Health. 35 (2004) 1.
- 14. Kaewpradit, C., Triampo, W., Tang, I.M. Limit Cycle of a Herbuvire-plantbee Model Containing a Time Delay. *ScienceAsia*. **31** (2005) 193.

Subproject 4

- Tiensuwan, M.; Yimprayoon, P.; Lenbury, Y. Application of Log-linear Models to Cancer Patients: A Case Study of Data from the National Cancer Institute of Thailand, submitted to Southeast Asian Journal of Tropical Medicine and Public Health.
- Tiensuwan, M., Rattanapornpong, S., Lenbury, Y. Applications of Logistic Regression Models to Cancer Patients: A Case Study of the National Cancer Institute. (In preparation).

Subproject 5

 Triampo, W., Doungchawee, G., Triampo, D., Wong-Ekkabut, J., Tang, I.M. Effects of Static Magnetic Field on Growth of Leptospire, Leptospira interrogans serovar canicola: Immunoreactivity and Cell Division. Journal of Bioscience and Bioengineering. 98(3) (2004) 182-186.

- Ngamsaad, W., Triampo, W., Kanthang, P., Modchang, C., Nuttavut, N., Tang, I.M., Lenbury, Y. A Lattice Boltzann Method for Modeling the Dynamic Pole-to-pole Oscillations of Min Proteins for Determining the Position of the Midcell Division Plane. J. Korean Phys. Soc. 46(4) (2005) 1025-1030.
- Modchang, C., Kanthang, P., Triampo, W., Ngamsaad, W., Nuttavut, N., Tang, I.M., Lenbury, Y. Modeling of the Dynamic Pole-to-pole Oscillations of the *Min* Proteins in Bacterial Cell Division: The Effect of an External Field. J. Korean Phys. Soc. 46(4) (2005) 1031-1036.

Subproject 6

1

Ž,

ę.

£ .

1

1

ķ

ŧ

4

- Kaewong, T., Niamsup, P., Lenbury, Y. A Note on Asymptotic Stability Conditions for Delay Difference Equations. *International Journal of Mathematics and Mathematical Sciences*. 7 (2005), 1007-1013.
- Plienpanich, T., Niamsup, P., Lenbury, Y. Controllability and Stability of the Perturbed Chen Chaotic Dynamical System. Applied Mathematics and Computations. In Press.
- 3. Niamsup, P., Lenbury, Y. The Asymptotic Stability of $x_{n+1} a^2 x_{n-1} + b x_{n-k} = 0$, accepted in *Kyungpook Mathematical Journal*. (under minor revision).
- 4. Niamsup, P., Lenbury, Y. M, -Factors and Q, -Factors for Near Quasi-Norm on Certain Sequence Spaces, to appear in to *International Journal of Mathematics and Mathematical Sciences*, 2005.

7.4 Publications output of P.I. (Prof. Y. Lenbury) in last 3 years

- 30. Kunphasuruang, W., Lenbury, Y., Hek, G. A Nonlinear Mathematical Model for Pulsatile Discharges of Luteinizing Hormone Mediated by Hypothalamic and Extra-Hypothalamic Pathways. *Mathematical Models* and Methods in Applied Sciences. 12(5) (2002) 607-624. (Impact factor 0.816)
- 31. Dumrongpokaphan, T., Lenbury, Y. Cascade Mechanism in a Self-regulatory Endocrine System: Modelling Pulsatile Hormone Secretion. *Pure and Applied Chemistry.* **74(6)** (2002) 881-890. (Impact factor 1.750)

- 32. Lenbury, Y., Pansuwan, A., Tumrasvin, N. Chaos and Control Action in a Kolmogorov Type Model for Food Webs with Harvesting or Replenishment. *ScienceAsia*. **28(3)** (2002) 205-215. (Impact factor 0.06)
- 33. Suwanwongse, S., Chasreechai, S., Lenbury, Y., Kataunyuthita, S. Modeling of AIDS Incidence and the Response of Transmission Rates to Increased Awareness: a Case Study of the Thai Province of Nakorn Pathom. Southeast Asian Journal of Tropical Medicine and Public Health. 33(3) (2002) 581-588. (Impact factor 0.097)
- 34. Siripunvaraporn, W., Egbert, G., Lenbury, Y. Numerical Accuracy of Magnetotelluric Modeling: A Comparison of Finite Difference Approximations. *Earth Planets and Space*. **54(6)** (2002) 721-725. (Impact factor 0.822)
- Pongsumpun, P., Lenbury, Y., Tang, I.M. Age Structure in a Model for the Transmission of Dengue Haemorrhagic Fever in Thailand. *East-West Journal of Mathematics*. Special Volume (2002) 93-103. (Reviewed by Math. Review)
- 36. Kammanee, A., Lenbury, Y., Tang, I.M. Transmission of *Plasmodium Vivax* Malaria. *East-West Journal of Mathematics*. **Special Volume** (2002) 277-284. (Reviewed by Math. Review)
- 37. Kanyamee, N., Lenbury, Y., Tang, I.M. The Effect of Migrant Workers on the Transmission of Malaria. *East-West Journal of Mathematics*. **Special Volume** (2002) 297-308. (Reviewed by Math. Review)
- Rattanakul, C., Lenbury, Y., Krishnamara, N., Wollkind, D.J. Modeling of Bone Formation and Resorption Mediated by Parathyroid Hormone: Response to Estrogen/PTH Therapy. *BioSystems*. 70(1) (2003) 55-72. (Impact factor 0.846)
- 39. Maneesawarng, C., Lenbury, Y. Total Curvature and Length Estimate for Curves in CAT(K) spaces. *Differential Geometry and its Applications*. 19 (2003) 211-222. (Impact factor 0.704)
- 40. Dumrongpokaphan, T., Lenbury, Y., Crooke, P.S. The Analysis of Higher-Order Cascade Systems with Separation Conditions Pivoting on the Slow Components: Application to a Model of Migration for Survival of the Species. *Mathematical and Computer Modelling*. 38 (2003) 671-690. (Impact factor 0.426)

41. Triampo, W., Triampo, D., Tang, I.M., Lenbury, Y. Random Walk on a Plane-Spin-Rotator System: Continuum Theory and Monte Carlo Simulations. *ScienceAsia*. **29** (2003) 289-299. (Impact factor 0.06)

pt 2

抻

e k

ħį

į

1

- 42. Wong-ekabut, J., Triampo, W., Tang, I.M., Triampo, D., Baowan, D., Lenbury, Y., Vacancy-Mediated Disordering Process in Binary Alloys at Finite Temperatures: Monte Carlo Simulation. *Journal of the Korean Physical Society*. **45(2)** (2004) 310-317. (Impact factor 0.505)
- 43. Poltem, D., Wiwatanapataphee, B., Ruengsakulrach, P., Lenbury, Y., Punpocha, M., Wu, Y.H. A Numerical Study of Blood Flow Patterns in Coronary Artery Bypass Grafts. *Quantitative Methods*. **1(1)** (2004) 1-7.
- 44. Lenbury, Y., Giang, D.V. Nonlinear Delay Differential Equations Involving Population Growth. *Mathematical and Computer Modelling*. **40** (2004) 586-590. (Impact factor 0.426)
- 45. Lenbury, Y., Pornsaward, P. A Delay-differential Equation Model of the Feedback-controlled Hypothalamus-pituitary-adrenal Axis in Humans. *Mathematical Medicine and Biology: A Journal of the IMA*. **22** (2005) 15-33.
- Crooke, P.S., Kongkul, K., Lenbury, Y., Adams, A.B., Carter, C.S., Marini, J.J., Hotchkiss, J.R. Mathematical Models for Pressure Controlled Ventilation of Oleic Acid-injured Pigs. *Mathematical Medicine and Biology.* 22 (2005) 99-112.
- Giang, D.V., Lenbury, Y., Seidman, T.I. Delay Effect in Models of Population Growth. *Journal of Mathematical Analysis and Applications*.
 305 (2005) 631-643. (Impact factor 0.458)
- 48. Siripunvaraporn, W., Egbert, G., Lenbury, Y., Uyeshima, M. Three-Dimension Magnetotelluric Inversion: Data Space Method. *Physics of the Earth and Planetary Interiors*. **150** (2005) 3-14. (Impact factor 1.246)
- 49. Ngamsaad, W., Triampo, W., Kanthang, P., Tang, I.M., Nuttawut, N., Modjung, C., Lenbury, Y. A Lattice Boltzmann Method for Modeling the Dynamic Pole-to-Pole Oscillations of Min Proteins for Determining the Position of the Midcell Division Plane. *Journal of the Korean Physical Society*. 46(4) (2005) 1025-1030. (Impact factor 0.790)
- 50. Modchang, C., Kanthang, P., Triampo, W., Ngamsaad, W., Nuttawut, N., Tang, I.M., Sanguansin, S., Boondirek, A., Lenbury, Y. Modeling of the

- 50. Modchang, C., Kanthang, P., Triampo, W., Ngamsaad, W., Nuttawut, N., Tang, I.M., Sanguansin, S., Boondirek, A., Lenbury, Y. Modeling of the Dynamic Pole-to-Pole Oscillations of the Min Proteins in Bacterial Cell Division: the Effect of an External Field. *Journal of the Korean Physical Society*. 46(4) (2005) 1031-1036. (Impact factor 0.790)
- Kaewong, T., Lenbury, Y., Niamsup, P. A Note on Asymptotic Stability Conditions for Delay Difference Equations. *International Journal of Mathematics and Mathematical Sciences*. 7 (2005) 1007-1013.
- 52. Pansuwan, A., Rattanakul, C., Lenbury, Y., Wollkind, D.J., Harrison, L., Rajapakse, I. Nonlinear Stability Analyses of Pattern Formation on Solid Surfaces During Ion-Sputtered Erosion. *Mathematical and Computer Modelling*. In Press. (Impact factor 0.426)
- Plienpanich, T., Niamsup, P., Lenbury, Y. Controllability and Stability of the Perturbed Chen Chaotic Dynamical System. *Applied Mathematics and Computations*. In Press. (Impact factor 0.359)
- 54. Yanarojana, S., Chantharaksria, U., Wilairat, P., Lenbury, Y. Kinetic Modeling of Lipoprotein Peroxidation Initiated by Copper and Azo Compounds. Science Asia. In Press. (Impact factor 0.06)

7.5 Names of graduated students

7.5.1 Ph.D. students

Subproject 1

- 1. Rujira Ouncharoen
- 2. Thongchai Dumrongpokaphan
- 3. Chontita Rattanakul
- 4. Konvika Kongkul
- 5. Sahattaya Rattanamongkonkul
- 6. Adoon Pansuwan

Subproject 2

- 1. Jutatip Archapitak
- 2. Bundit Unyong

Subproject 3

- 1. Puntani Pongsumpun
- 2. Surapol Noaowarat

- 3. Malee Sriprom
- 4. Somporn Punpocha

7.5.2 Master students

Subproject 1

1. Pornsup Pornsawad

Subproject 2

1. Sineenart Srimongkol

Subproject 3

jŀ

ŧļ.

.

- 1. Ratchanee Muangyai
- 2. Somchai Sriyab
- 3. Charn Khetchaturat
- 4. Kot Patanarapelert
- 5. Athassawat Kammanee
- 6. Nairat Kanyamee
- 7. Weerachai Sarakorn
- 8. Charn Khetchaturat
- 9. Eakchai Navapunyakul

Subproject 4

- 1. Sompit Thammasurat
- 2. Ngamphol Sunthornworasiri
- 3. Sugunya Rattanapornpong

Subproject 6

- 1. Jutarat Kongson
- 2. Teeranush Suebcharoen
- 3. Tidarut Plienpanich
- 4. Kreangkri Ratchgit
- 5. Thongchai Botmart
- 6. Thasanai Chamnanpet

8. ADDITIONAL COMMENTS

Two annual progress report meetings have been organized.

8.1 First annual meeting: May 8-9, 2003

The program

- i) 2 invited lectures by Prof. Yuesheng Xu form West Verginia University.
- ii) 13 contributed papers.

Attendance

- i) On May 8, 86 participants.On May 9, 61 participants.
- ii) Participants were from 16 universities.
- 8.2 Second annual meeting: January 7-8, 2004.

The program

- i) 4 invited lectures by
 - Prof. Charles Micchelli from University at Albany, New York, U.S.A.
 - Prof. Hideaki Kaneko from Old Dominion University, Virginia, U.S.A.
 - Asst. Prof. Massimiliano Pontil from University College, London, U.K.
 - Assoc. Prof. Wayne Michael Lawton from National University of Singapore,
 Singapore.
- ii) 7 contributed papers.

Attendance

- i) On January 7, 55 participants.On January 8, 58 participants.
- ii) Participants were from 11 universities.
- 8.3 The final report meeting is being organized as an international conference (ICMA-MU 2005) during December 15-17, 2005. Announcement has been posted in the web (www.sc.mahidol.ac.th/scma/).

9. APPENDICES

9.1 Manuscripts of newly accepted / appeared papers

Subproject 1 pages 108-219

- 1.1 Dumrongpokaphan, T., Lenbury, Y., Crooke, P.S. The Analysis of Higher-Order Cascade Systems with Separation Conditions Pivoting on the Slow Components: Application to a Model of Migration for Survival of the Species. *Mathematical and Computer Modelling*. 38 (2003) 671-690.
- 1.2 Giang, D.V., Lenbury, Y., Seidman, T.I. Delay Effect in Models of Population Growth. *Journal of Mathematical Analysis and Applications*. 305 (2005) 631-643.
- 1.3 Lenbury, Y., Giang, D.V. Nonlinear Delay Differential Equations Involving Population Growth. *Mathematical and Computer Modelling*. **40** (2004) 586-590.

- 1.4 Lenbury, Y., Pansuwan, A., Tumrasvin, N. Chaos and Control Action in a Kolmogorov Type Model for Food Webs with Harvesting or Replenishment. Science Asia. 28(3) (2002) 205-215.
- 1.5 Rattanakul, C., Lenbury, Y., Krishnamara, N., Wollkind, D.J. Modeling of Bone Formation and Resorption Mediated by Parathyroid Hormone: Response to Estrogen/PTH Therapy. *BioSystems*. 70(1) (2003) 55-72.
- 1.6 Lenbury, Y., Pornsaward, P. A Delay-differential Equation Model of the Feedback-controlled Hypothalamus-pituitary-adrenal Axis in Humans. Mathematical Medicine and Biology: A Journal of the IMA. 22 (2005) 15-33.

ij

li

- 1.7 Dumrongpokaphan, T., Lenbury, Y. Cascade Mechanism in a Self-regulatory Endocrine System: Modelling Pulsatile Hormone Secretion. *Pure and Applied Chemistry*. 74(6) (2002) 881-890.
- 1.8 Crooke, P.S., Kongkul, K., Lenbury, Y., Adams, A.B., Carter, C.S., Marini, J.J., Hotchkiss, J.R. Mathematical Models for Pressure Controlled Ventilation of Oleic Acid-injured Pigs. *Mathematical Medicine and Biology.* 22 (2005) 99-112.

Subproject 2 pages 220-224

2.1 Poltem, D., Wiwatanapataphee, B., Ruengsakulrach, P., Lenbury, Y., Punpocha, M., Wu, Y.H. A Numerical Study of Blood Flow Patterns in Coronary Artery Bypass Grafts. *Quantitative Methods*. 1(1) (2004) 1-7.

Subproject 3 pages 225-341

- 3.1 Pongsumpun, P., Yoksan, S., Tang, I.M. A Comparison of the Age Distributions in the Dengue Hemorrhagic Fever Epidemics in Santiago de Cuba (1997) and Thailand (1998). Southeast Asian Journal of Tropical Medicine and Public Health. 33 (2002) 255.
- 3.2 Pongsumpun, P., Lenbury, Y., Tang, I.M. Age Structure in a Model for the Transmission of Dengue Hemorrhagic Fever in Thailand. *East-West Journal of Mathematics*. **Special Volume** (2002) 93-103.
- 3.3 Kammanee, A., Lenbury, Y., Tang, I.M. Transmission of Plasmodium Vivax Malaria. East-West Journal of Mathematics. Special Volume (2002) 277-284.

- 3.4 Kanyamee, N., Lenbury, Y., Tang, I.M. The Effect of Migrant Workers on the Transmission of Malaria. East-West Journal of Mathematics. Special Volume (2002) 297-308.
- 3.5 Pongsumpun, P., Tang, I.M. Transmission of Dengue Hemorrhagic Fever in an Age Structured Population. *Math. Comp. Model.* **37** (2003) 949-961.
- 3.6 Kaewmanee, C., Tang, I.M. Cannibalism in an Age-structured Predator-prey System. *Ecol. Modelling* **167** (2003) 213-220.
- 3.7 Sriprom, M., Pongsumpun, P., Yoksan, S., Barbazan, P., Gonzales, J.P., Tang, I.M. Dengue Haemorrhagic Fever in Thailand 1998-2003: Primary or Secondary. *Dengue Bulletin.* 27 (2003) 39-45.
- 3.8 Nishiura, H., Tang, I.M., Kakehashi, M. The Impact of Initial Attack Size on Sars Epidemic for SARS Free Countries: Possible Reason for Japan without a Domestic Transmission. *Journal of Medical Safety*. **1(1)** (2003) e1-e6.
- 3.9 Pongsumpun, P., Patanarapelert, K., Sriprom, M., Varamit, S., Tang, I.M. Infection Risk to Travellers Going to Dengue Fever Regions. Southeast Asian Journal of Tropical Medicine and Public Health. 35 (2004) 155.
- 3.10 Naowarat, S., Tang, I.M. Effect of Bird-to-bird Transmission of the West Nile Virus on the Dynamics of the Transmission of this Disease. Southeast Asian Journal of Tropical Medicine and Public Health. 35 (2004) 162.
- 3.11 Nishiura, H., Patanaraspelert, K., Sriprom, M., Sarakorn, W., Sriyab, S., Tang, I.M. Modelling Potential Responses to Severe Acute Respiratory Syndrome (SARS) in Japan: the Role of Initial Attack Size, Precaution and Quarantine. J. Epid. Commun. Health. 58(3) (2004) 156.
- 3.12 Nishiura, H., Tang, I.M. Modeling for a Smallpox-vaccination Policy against Possible Bio-terrorism in Japan: The Impact of Long-lasting Vaccinal Immunity. J. Epid. 14(2) (2004) 41.
- 3.13 Nishiura, H., Patanarapelert, K., Khortwong, P., Tang, I.M., Pasakorn, A. Predicting the Future Trend of Drug-resistant Tuberculosis in Thailand: Assessing the Impact of Control Strategy. Southeast Asian Journal of Tropical Medicine and Public Health. 35 (2004) 1.
- 3.14 Kaewpradit, C., Triampo, W., Tang, I.M. Limit Cycle of a Herbuvire-plant-bee Model Containing a Time Delay. *ScienceAsia*. **31** (2005) 193.

Subproject 5 pages 342-358

5.1 Triampo, W., Doungchawee, G., Triampo, D., Wong-Ekkabut, J., Tang, I.M. Effects of Static Magnetic Field on Growth of Leptospire, Leptospira interrogans serovar canicola: Immunoreactivity and Cell Division. Journal of Bioscience and Bioengineering. 98(3) (2004) 182-186.

- 5.2 Ngamsaad, W., Triampo, W., Kanthang, P., Modchang, C., Nuttavut, N., Tang, I.M., Lenbury, Y. A Lattice Boltzann Method for Modeling the Dynamic Pole-to-pole Oscillations of Min Proteins for Determining the Position of the Midcell Division Plane. *Journal of the Korean Physical Society.* 46(4) (2005) 1025-1030.
- 5.3 Modchang, C., Kanthang, P., Triampo, W., Ngamsaad, W., Nuttavut, N., Tang, I.M., Lenbury, Y. Modeling of the Dynamic Pole-to-pole Oscillations of the Min Proteins in Bacterial Cell Division: The Effect of an External Field. Journal of the Korean Physical Society. 46(4) (2005) 1031-1036.

Subproject 6 pages 359-393

- 6.1 Kaewong, T., Niamsup, P., Lenbury, Y. A Note on Asymptotic Stability Conditions for Delay Difference Equations. *International Journal of Mathematics and Mathematical Sciences*. 7 (2005), 1007-1013.
- 6.2 Plienpanich, T., Niamsup, P., Lenbury, Y. Controllability and Stability of the Perturbed Chen Chaotic Dynamical System. Applied Mathematics and Computations. In Press.
- 6.3 Niamsup, P., Lenbury, Y. The Asymptotic Stability of $x_{n+1} a^2 x_{n-1} + b x_{n-k} = 0$, accepted in *Kyungpook Mathematical Journal*. (under minor revision).
- 6.4 Niamsup, P., Lenbury, Y. M, Factors and Q, Factors for Near Quasi-Norm on Certain Sequence Spaces, to appear in to International Journal of Mathematics and Mathematical Sciences, 2005.

9.2 Announcements of Special Seminars

111 seminars have been organized by members of the project in the past 3 years.

(Appendix # 7) pages 394-452

Signature

Prof. Yongwimon Lenbury

(Project Leader)



Mathematical and Computer Modelling 38 (2003) 671-690

MATHEMATICAL AND COMPUTER MODELLING

www.elsevier.com/locate/mcm

The Analysis of Higher-Order Cascade Systems with Separation Conditions Pivoting on the Slow Components: Application to a Model of Migration for Survival of the Species

T. DUMRONGPOKAPHAN AND Y. LENBURY*

Department of Mathematics
Faculty of Science, Mahidol University
Bangkok, Thailand

P. S. CROOKE

Department of Mathematics, Vanderbilt University Nashville, TN 37240, U.S.A.

(Received August 2001; accepted August 2002)

Abstract—Cascade systems, characterized by highly diversified time responses, are considered in this paper. Singular perturbation principles, which have been used to analyze relaxation oscillations in second-order dynamical systems, will be extended here to accommodate nonlinear systems in which more state variables are involved in multiscale interactions. Separation conditions will be derived for the identification of limit cycle behavior in a higher-dimensional $(n \ge 4)$ cascade system. It is found that when appropriate regularity and boundedness requirements are met by the slow components of the dynamical system, pivoting on the slow components can lead to separation conditions which identify limit cycle behavior as well as other dynamic behavior permitted by the model. The principle is then applied to a model of two communities coupled by migration. Through such analysis, we can examine how the mechanisms of migration, variations in reproduction, recruitment, mortality, and feeding success, exploited by interacting species, may achieve survival and coexistence of the populations concerned. © 2003 Elsevier Ltd. All rights reserved.

Keywords—Cascade systems, Singular perturbation, Sustained oscillation, Persistence, Migration.

INTRODUCTION

Several important cascade systems are found in nature which incorporate some form of diversities in their dynamics. Many endocrine systems are considered to constitute a cascade mechanism for being an amplification system where an initial reaction gives rise to the generation of multiple second reactions, each of which sets off multiple third reactions, and so on.

^{*}Author to whom all correspondence should be addressed.

Deepest appreciation is extended to the Thailand Research Fund for the financial support (Contract Numbers RTA/02/2542 and PHD/0029/2543).

An example of endocrine cascade systems involves the hypothalamus, pituitary, and distal endocrine secreting glands. A signal, in either the external or internal environment, is sent to the limbic system and then the hypothalamus, resulting in the secretion of a releasing hormone into the closed portal system connecting the hypothalamus and anterior pituitary. Releasing hormones may be secreted in nanogram amounts and have half-lives of about 3–7 min [1]. They then stimulate the release of the appropriate anterior pituitary hormones, which may be secreted in microgram amounts with half-lives on the order of 20 min or longer. These hormones in turn signal the secretion of the ultimate hormones, which may be secreted in many micrograms or milligrams and may be fairly stable. Thus, the stability and amounts of the hormones increase as one proceeds down the cascade.

Such cascade effects can be found also in ecosystems, in the majority of food chains where the size and time needed for reproduction and growth of the individuals of each population are increasing with the trophic levels. Phytoplankton-zooplankton-fish is a typical example [2]. In fact, almost all food chains belonging to the class vegetation-herbivore-carnivore have time responses increasing along the chain from bottom to top, an exception of which is the chain "tree-defoliator-bird" in which the second trophic level is that with the fastest dynamics [2].

It is well known that such systems characterized by highly diversified dynamics can be analyzed with the singular perturbation method [2], under suitable regularity assumptions. Such arguments have been used to analyze relaxation oscillations in slow-fast second-order dynamical systems and have been extended successfully to apply to three-dimensional systems by Muratori and Rinaldi [3]. However, in a complex system where more than three state variables are involved, analysis and identification of sustained oscillation become a formidable task. Since a great deal of understanding and insights can be gained from such analysis which cannot be achieved from numerical work alone, we attempt here to extend the concept to accommodate higher-dimensional systems. Lenbury et al. [4] was able to derive the separation condition for a higher-dimensional system by pivoting about the fast components of the system, upon certain assumptions of their boundedness and regularity. Here, we show that in a different circumstance where pivoting about the slow components is allowed, existence of sustained oscillations may be ascertained at relative ease through the singular perturbation analysis. We derive the separation and delineating conditions, which help us to identify different dynamical behavior permitted by a nonlinear system of order greater than or equal to four.

Application is then made to a model of predator-prey communities coupled by migration in order to investigate how certain species can survive by exploiting the mechanisms which involve a combination of migration, variations in rates of reproduction, consumption, and mortality.

According to Matsumoto and Seno [5], population persistence is influenced by both biotic and abiotic environmental heterogeneity, namely, resource distribution, temperature, humidity, stochastic disturbance, and so on. Some effect of local environmental heterogeneity is transferred through population migration processes and affects the whole population to affect population persistence.

Whitehead [6], in his report on the variation in the feeding success of sperm whales, stated that a consideration of scale should be central in ecology. At the species level, patterns of environmental variation over a wide range of spatial and temporal scales determine population ecology and define evolutionary selective pressure. "Populations of particular species track spatial and temporal variability in their environment at some scales but not others. Tracking at temporal scales longer than the organism's lifetime and spatial scales broader than its home range is largely achieved through variations in reproduction, recruitment, mortality, and migration." Environmental variability over smaller scales usually results in changes in the feeding success, nutritional status, and, sometimes, the behavior of individual organisms.

Whitehead's study [6] found that sperm whales maintain high biomass and very low reproductive rates in an environment which shows great variability over time scales of one or more years. As the environmental variation has little coherence over scales of about 300 km or more, the study

found that sperm whales are able to use migration as their principal strategy for surviving in an uncertain habitat. During periods characterized by low feeding success groups of sperm whales moved greater distances and are able to maintain high biomass and low reproductive rates in an environment which, at any location, contains long, unpredictable periods of food shortage. Groups have been found to move more consistently in particular directions when feeding success is low, and doubling back on their tracks when it is high.

Walde [7] also presented field data which indicated that population densities were higher and persistence was greater where immigration rates were higher. Most importantly, it appeared that temporal patterns of density and, perhaps, probability of persistence, were dependent on the amount of migration between populations.

As commented by Walde [7], most of the current debate is centered on the question of the mechanisms underlying the stability among interacting species. One of the two alternative hypotheses in such a debate is that the predator-prey interaction is stable at a relatively small spatial scale due to mechanisms such as foraging behavior, or due to fine-scale physical biotic heterogeneity. The other hypothesis is that the interaction is stable at a larger spatial scale due to migration among partially subdivided populations.

We, therefore, study a simple model of two communities, assuming that predators can migrate between communities, while prey cannot. Prey populations in the two communities are assumed to exhibit different reproductive behavior to take into account the difference in abundance, and different parameters are assigned to the predators response functions to model the variation in the foraging success in the two communities. The condition for migration is the difference in predator population densities. We derive the higher-dimensional separation conditions developed in this paper to identify limit cycle behavior and carry out an analysis of the dynamics of the four-dimensional model in order to provide partial support for the arguments concerning the stability of the system and the persistence of the populations in the coupled communities.

Singular Perturbation Arguments in the Lower-Dimensional Case

In order to understand how the singular perturbation arguments can be used to detect limit cycles in a three component cascade system, let us consider a third-order system of the form

$$\dot{x} = f(x, y, z; \alpha),\tag{1}$$

$$\dot{y} = \varepsilon g(x, y, z; \alpha),\tag{2}$$

$$\dot{z} = \varepsilon \delta h(x, y, z; \alpha),\tag{3}$$

where ε and δ are small positive parameters. Thus, when the right sides of equations (1)-(3) are finite and different from zero, $|\dot{y}|$ is of the order ε and $|\dot{z}|$ is of the order $\varepsilon\delta$. Therefore, x is the fast variable, z is the slow one, while y has intermediate dynamics.

As explained by Muratori and Rinaldi [2,3], system (1)–(3) with small ε and δ can be analyzed with the singular perturbation method which, under suitable regularity conditions, allows approximating the solution of system (1)–(3) with a sequence of simple dynamic transitions occurring at different speeds. The argument, following that of Muratori and Rinaldi's [2,3], goes as follows.

Given an initial condition (x(0), y(0), z(0)), the slow z and intermediate (y) variables are frozen, and the "fast system"

$$\dot{x}(\tau_1) = f(x(\tau_1), y(0), z(0); \alpha), \qquad \tau_1 = \frac{t}{\varepsilon \delta}$$

$$(4)$$

is considered with initial condition x(0). Thus, the fast component x varies very quickly according to equation (4), and eventually tends toward a stable equilibrium $\bar{x}(x(0), y(0), z(0))$ of (4). Then, still keeping z frozen at z(0), we now consider the "intermediate system"

$$\dot{y}(\tau_2) = g(\bar{x}(x(0), y(\tau_2), z(0)), y(\tau_2), z(0); \alpha), \qquad \tau_2 = \frac{t}{\delta}.$$
 (5)

where $\ddot{x}(x(0),y,z(0))$ is a stable equilibrium of the fast system (4) with y(0) replaced by y.

Referring to Figure 1, where slow, intermediate, and high-speed transitions are indicated, respectively, by one, two, and three arrows, a transition at high speed $(\tau_1 = t/\varepsilon\delta)$ first develops at constant y and z and brings the system from the point (x(0), y(0), z(0)), point A in Figure 1, to point B on a stable equilibrium of the slow manifold f = 0. Then a second intermediate speed $(\tau_2 = t/\delta)$ transition is made on the manifold at constant z until an equilibrium $\bar{y}(x(0), y(0), z(0))$ of system (5) is approached (point C in Figure 1). A third transition then follows at low speed along the line obtained by intersecting the slow manifold f = 0 and the intermediate manifold g = 0. The transition may end at an equilibrium point where f = g = h = 0 or a situation may occur in which the stability of the manifold f = 0 is lost first at a bifurcation point f = 0 in Figure 1). Then, a fast catastrophic transition may bring the state of the system to a point on the other stable branch of the manifold f = 0 (point f = 0).

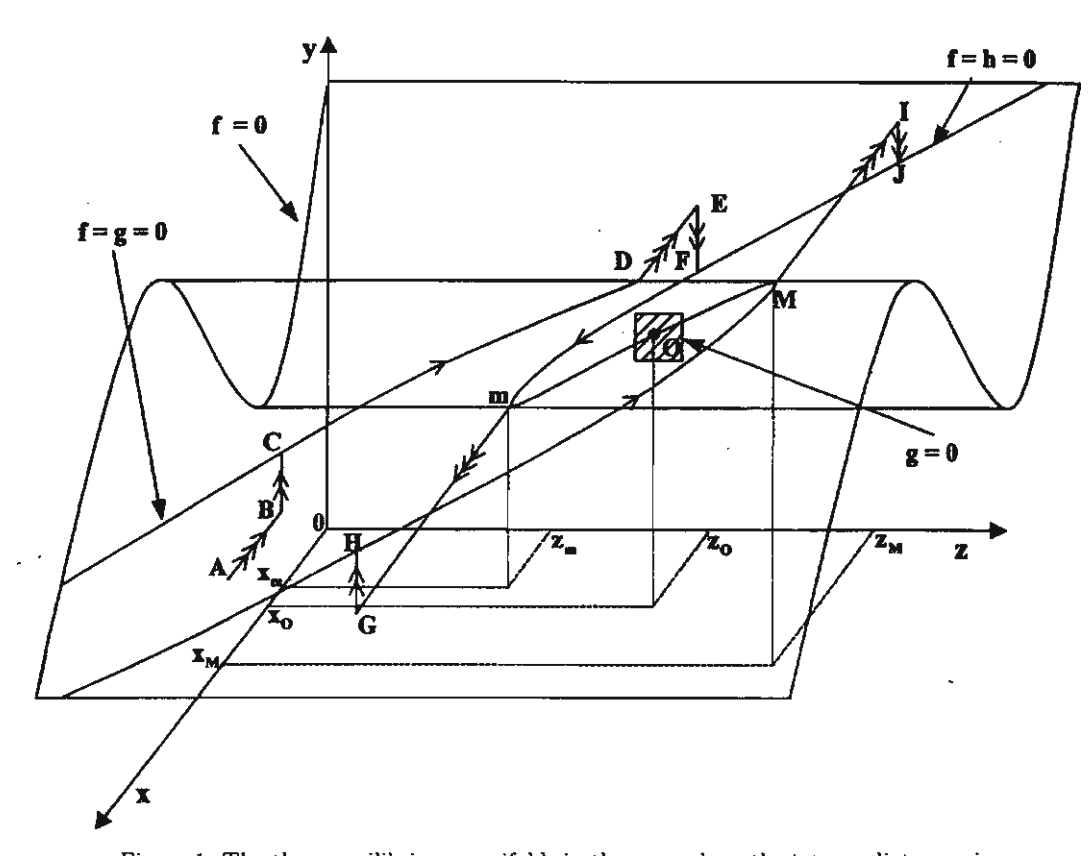


Figure 1. The three equilibrium manifolds in the case where the intermediate manifold g=0 separates the two stable branches of the curve f=h=0.

Now, if the manifold g=0 is positioned in such a way that point O, where f=g=h=0, is located between the two bifurcation points m and M on the curve f=h=0 so that the manifold g=0 separates the two stable branches of the curve as shown in Figure 1, then g>0 on one branch (the front one in Figure 1) and g<0 on the other (the back one).

In this case, once the system reaches point E, a transition develops at intermediate speed downward towards point F located on the intersection between f=0 and h=0 and follows this curve at slow speed in the direction of decreasing g until the bifurcation point g is reached. A catastrophic transition then brings the system to point g on the front part of g of followed by a transition at intermediate speed to point g on the front part of g of a slow transition will develop in the direction of increasing g until the stability of the manifold is lost again at point g on the first point g on the back portion of g of the system to point g on the back portion of g of g is now negative. A transition at intermediate speed then develops downward until point g on g is reached. A slow transition then follows along this curve until g is reached again. A quick jump to g closes up the cycle g and g is intermediate speed.

Obviously, the cycle can be much more complex if, for suitable values of its parameters, system (1)-(3) has multiple equilibria. However, we shall assume that for appropriately chosen parametric values, the manifold g=0 intersects the curve f=h=0 at only one point, namely the point $O(x_O,y_O,z_O)$ and the two bifurcation points on f=h=0 are $M(x_M,y_M,z_M)$ and $m(x_m,y_m,z_m)$. Then if, for a particular value of the system parameter α , the separation condition

$$x_m < x_O < x_M \tag{6}$$

holds, then the system of equations (1)-(3) has a stable limit cycle which is contained in a tube around the transitions described above, and the radius of the tube goes to zero with ε and δ .

Extension to Higher-Dimensional Systems Pivoting about the Slow Components

In order to extend the above concept to higher-dimensional systems, let us consider a system of n+3 differential equations which may be written in the form

$$\dot{x} = f(x, y, z, w; \alpha), \tag{7}$$

$$\dot{y} = \varepsilon g(x, y, z, w; \alpha), \tag{8}$$

$$\dot{z} = \varepsilon \delta h(x, y, z, w; \alpha), \tag{9}$$

$$\dot{w} = \varepsilon \delta \eta k(x, y, z, w; \alpha), \tag{10}$$

where ε , δ , and η are small positive constants, $\alpha \in \mathbb{R}^N$ is the N-dimensional vector of system parameters, while

 $\begin{bmatrix} x \\ y \\ z \end{bmatrix} \in \Re^3$

and

$$w = \begin{bmatrix} w_1 \\ w_2 \\ \vdots \\ w_n \end{bmatrix} \in \Re^n$$

are the n+3 state variables, and

$$k = \begin{bmatrix} k_1(x, y, z, w; \alpha) \\ k_2(x, y, z, w; \alpha) \\ \vdots \\ k_n(x, y, z, w; \alpha) \end{bmatrix}.$$

Hence, x is the fast variable, y the intermediate, z the slow, and w_i , i = 1, 2, ..., n, the very slow components of the system.

Employing the same line of arguments as above, we first assume that w is varying extremely slowly in comparison to the first three components x, y, and z. Then, we may initially assume that w is kept frozen at a constant value w(0) while x, y, and z vary according to the three-dimensional system

$$\dot{x} = f(x, y, z, w(0); \alpha), \tag{11}$$

$$\dot{y} = \varepsilon g(x, y, z, w(0); \alpha), \tag{12}$$

$$\dot{z} = \varepsilon \delta h(x, y, z, w(0); \alpha). \tag{13}$$

Thus, if, for suitable parametric values α , the relative positions of the three equilibrium manifolds of system (11)-(13) are the same as those three shown in Figure 1, then trajectories will

develop as described earlier. However, as w varies with time, though very slowly, the shapes and positions of the three manifolds shift slowly as time passes. The coordinates of points m, M, and O are, in this case, $(x_m(w;\alpha), y_m(w;\alpha), z_m(w;\alpha))$, $(x_M(w;\alpha), y_M(w;\alpha), z_M(w;\alpha))$, and $(x_O(w;\alpha), y_O(w;\alpha), z_O(w;\alpha))$, respectively, since f, g, and h are all functions of w.

Moreover, since w may not equilibrate and the manifolds $k_i(x, y, z, w; \alpha) = 0$, i = 1, 2, ..., n, may not be stable, as the transitions develop around the curve shown in Figure 1, the value of w can swing about off the manifolds

$$k_i(x, y, z, w; \alpha) = 0, \qquad i = 1, 2, \dots, n.$$
 (14)

If we further assume that each of the equations in (14) can be solved for z as an explicit function of the other components

$$z = Z_i(x, y, w; \alpha), \qquad i = 1, 2, \dots, n, \tag{15}$$

then we see that extra separation conditions are needed to ensure that the manifolds described by the equations in (15) are positioned in between the two stable branches of the curve f = h = 0 as well, in order that a limit cycle exists. These conditions are stated in the following theorem, under all the assumptions mentioned above.

THEOREM. Suppose that the functions $f(x, y, z, w; \alpha)$, $g(x, y, z, w; \alpha)$, $h(x, y, z, w; \alpha)$, and $k(x, y, z, w; \alpha)$ are continuous, and that the functions $x_M(w; \alpha)$, $z_M(w; \alpha)$, z

$$\sup_{w} x_m(w; \alpha) < \inf_{w} x_O(w; \alpha), \tag{16}$$

$$\sup_{w} x_{\mathcal{O}}(w; \alpha) < \inf_{w} x_{\mathcal{M}}(w; \alpha), \tag{17}$$

$$\sup_{w} z_{m}(w; \alpha) < \min_{i} \inf_{\Delta_{i}} Z_{i}, \tag{18}$$

$$\max_{i} \sup_{\alpha} Z_{i} < \inf_{w} z_{M}(w; \alpha), \tag{19}$$

where the supremum and infemum of Z_i are taken over its domain Δ_i which is a subset of \Re^{n+2} , then a limit cycle exists for the system of equations (7)-(10), provided that ε , δ , and η are sufficiently small.

PROOF. Since the functions involved are assumed to be bounded in their respective domains, the infema and suprema in inequalities (16)–(19) exist. The separating conditions (16),(17) and the continuity of the functions concerned guarantee that, as w ranges over time, the intermediate equilibrium manifold g=0 will remain in the appropriate position, separating the two stable branches of the submanifold f=h=0, under the regularity assumptions already mentioned above. The transitions will develop as shown in Figure 1, even as w varies slowly. The separation conditions (18) and (19) ensure that, as the transition reaches the highest value of z at point M in Figure 1, which keeps shifting with w, the trajectory in the (n+3)-dimensional space swings to one side of the manifolds given by (15), and when the transition reaches the lowest value of z at point m in Figure 1, the trajectory has swung over to the other side of the manifolds given by (15). This guarantees that w shall not increase or decrease without bound, but remain close to the manifolds $z=Z_i$, $i=1,2,\ldots,n$, permitting sustained oscillation around a closed cycle as identified in Figure 1, provided that ε , δ , and η are sufficiently small.

APPLICATION TO A MODEL OF COMMUNITIES COUPLED BY MIGRATION

In order to illustrate how the technique can be applicable to practical situations, we consider a model of two predator-prey communities coupled by migration, consisting of the following

677

nonlinear differential equations:

$$\dot{x} = r_1 x (1 - x) - \frac{\gamma_1 x y}{x + M_1},\tag{20}$$

$$\dot{y} = \frac{C_1 \gamma_1 x y}{x + M_1} - D_1 y - \mu_1 (y - z), \tag{21}$$

$$\dot{z} = \frac{C_2 \Gamma_2 z w}{w + M_2} - D_2 z + \mu_2 (y - z), \tag{22}$$

$$\dot{w} = \frac{R_2 w}{w + r_3} - \frac{\Gamma_2 z w}{w + M_2},\tag{23}$$

where x, y, z, and w are the population densities of prey in the first community, predators in the first community, predators in the second community, and prey in the second community, respectively. The growth rate of prey in the first community is assumed to be logistic, while a saturation function is assumed for prey in the second community in order to incorporate the effect of resource variability in the two environments. Holling type response functions are assumed for both predators with conversion factors C_1 and C_2 specifying the numbers of newly born predators for each captured prey. Parameters γ_1 and Γ_2 are the maximum predation rates, M_1, M_2, r_3 the half-saturation constants, D_1, D_2 the corresponding death rates, and R_2 is the maximum birth rate of prey in the second community. Parameters μ_1 and μ_2 are the variation constants of migration from one community to the other, which are allowed to be different to account for the difference in spatial capacities available in the two habitats.

We assume that prey has very fast dynamics and the feeding success of the predators is higher in the first community. After a period of successful foraging, predator population density greatly increases while the level of prey continuously drops leading to shortage of food due to intrapopulation competition. Migration is then adopted as the predators' strategy for surviving in an uncertain habitat. The rate of migration from one community to the other is assumed to vary directly as the difference in the population densities. As Sherry observed in his recent study [8], habitats are considered saturated when some individuals are unable to secure or defend their ground due to competition, forcing settlement in less preferred areas. Thus, intraspecific competition in the first community may drive the predators to migrate to a less favorable habitat in which prey multiplies more slowly. However, evidence [6] shows that, confronted with low food availability, organisms may die, fast, or move. An adjustment in their reproductive rate and foraging behavior is a common strategy for survival in a less favorable environment and a decline of body mass is found in individuals occupying the most drought-stressed habitats. Therefore, predators in the second community are assigned slower dynamics than those in the first. Consequently, we scale the dynamics of the four components of the system by means of three small positive parameters ϵ , δ , and η as follows.

Letting $c_1 = C_1 \gamma_1/\varepsilon$, $d_1 = D_1/\varepsilon$, $v_1 = \mu_1/\varepsilon$, $c_2 = C_2 \Gamma_2/\varepsilon \delta$, $d_2 = D_2/\varepsilon \delta$, $v_2 = \mu_2/\varepsilon \delta$, $r_2 = R_2/\varepsilon \delta \eta$, and $\gamma_2 = \tau_2/\varepsilon \delta \eta$, we are led to the following model equations:

$$\dot{x} = r_1 x (1 - x) - \frac{\gamma_1 x y}{x + M_1} \equiv f(x, y, z, w), \tag{24}$$

$$\dot{y} = \varepsilon \left[\frac{c_1 x y}{x + M_1} - d_1 y - \upsilon_1(y - z) \right] \equiv \varepsilon g(x, y, z, w), \tag{25}$$

$$\dot{z} = \varepsilon \delta \left[\frac{c_1 z w}{w + M_2} - d_2 z + \upsilon_2 (y - z) \right] \equiv \varepsilon \delta h(x, y, z, w), \tag{26}$$

$$w = \varepsilon \delta \eta \left[\frac{r_2 w}{w + r_3} - \frac{\gamma_2 z w}{w + M_2} \right] \equiv \varepsilon \delta \eta k(x, y, z, w). \tag{27}$$

Thus, if ε , δ , and η are small, prey and predators in the first community have the fastest and intermediate dynamics, respectively. In the second community, the predator population has a relatively slow time response, while the prey population has the slowest dynamics.

We now study each of the equilibrium manifolds in detail.

The Manifold f = 0. This consists of the trivial manifold x = 0 and the nontrivial one given by the equation

$$y = \frac{r_1}{\gamma_1}(x + M_1)(1 - x), \tag{28}$$

which intersects the (y, z)-plane along the line

$$y=\frac{r_1}{\gamma_1}M_1.$$

The maximum point on this manifold is located at the point where

$$y = \frac{r_1(1+M_1)^2}{4\gamma_1} \equiv y_M \tag{29}$$

and

$$x = \frac{(1 - M_1)}{2} \equiv x_M,\tag{30}$$

as shown in Figure 2a.

THE MANIFOLD q = 0. This is the surface

$$z = \frac{y}{v_1} \left(d_1 + v_1 - \frac{c_1 x}{x + M_1} \right), \tag{31}$$

which intersects the trivial manifold x = 0 along the line

$$z = \frac{y}{v_1} (d_1 + v_1) \tag{32}$$

and intersects the nontrivial manifold f = 0 along the curve

$$z = \frac{r_1}{\gamma_1 \nu_1} (1 - x)((d_1 + \nu_1 - c_1)x + M_1(d_1 + \nu_1)). \tag{33}$$

Moreover, the curve f = g = 0 in (33) intersects the (x, y)-plane at the point where z = 0 and

$$x = \frac{M_1(d_1 + \nu_1)}{c_1 - (d_1 + \nu_1)} \equiv \hat{x},\tag{34}$$

which is positive provided that

$$c_1 > d_1 + v_1. (35)$$

The Manifold h = 0. This is a surface given by

$$z = \frac{\upsilon_2 y(w + M_2)}{(d_2 + \upsilon_2 - c_2)w + (d_2 + \upsilon_2)M_2},$$
(36)

which intersects the nontrivial manifold f = 0 along the curve given by

$$z = \frac{r_1 v_2}{\gamma_1} \left[\frac{(x + M_1)(1 - x)(w + M_2)}{(d_2 + v_2 - c_2)w + (d_2 + v_2)M_2} \right]. \tag{37}$$

The maximum point of the curve f = h = 0 in (37) is attained when $x = x_M$ given in (30) and, on substituting (30) into (37),

$$z = z_M(w) = \frac{r_1 \nu_2}{4\gamma_1} \left[\frac{(1+M_1)^2 (w+M_2)}{(d_2 + \nu_2 - c_2)w + (d_2 + \nu_2)M_2} \right].$$
(38)

Analysis of Higher-Order Cascade Systems

679

On differentiating $z_M(w)$, we find that

$$\frac{d}{dw}z_{M}(w)>0,$$

for all parametric values. Thus,

$$\inf_{w} z_{M}(w) = z_{M}(w)|_{w=0}$$

$$= \frac{r_{1}v_{2}(1+M_{1})^{2}}{4\gamma_{1}(d_{2}+v_{2})},$$
(39)

$$\sup_{w} z_{M}(w) = \lim_{w \to \infty} z_{M}(w)$$

$$= \frac{r_{1}v_{2}(1 + M_{1})^{2}}{4\gamma_{1}(d_{2} + v_{2} - c_{2})},$$
(40)

which is positive if

$$d_2 + v_2 > c_2. (41)$$

The point where the curve f = h = 0 in (37) intersects the (y, z)-plane is found by substituting x = 0 in (37), yielding

$$z = \frac{r_1 \nu_2 M_1(w + M_2)}{\gamma_1 \left[(d_2 + \nu_2 - c_2)w + (d_2 + \nu_2) M_2 \right]} \equiv z_m(w). \tag{42}$$

Differentiating $z_m(w)$, we find that

$$\frac{d}{dw}z_m(w) > 0,$$

for all parametric values. Thus,

$$\sup_{w} z_{m}(w) = \lim_{w \to \infty} z_{m}(w)
= \frac{r_{1}v_{2}M_{1}}{\gamma_{1}(d_{2} + v_{2} - c_{2})},$$
(43)

$$\inf_{w} z_{m}(w) = z_{m}(w)|_{w=0} = \frac{r_{1} \nu_{2} M_{1}}{\gamma_{1} (d_{2} + \nu_{2})},$$
(44)

which is always positive.

-

Finally, the curve f = g = 0 in (33) intersects the curve f = h = 0 in (37) at the point where $x = x_O(w)$ and

$$x_O(w) = \frac{M_1([(d_1+v_1)(d_2+v_2-c_2)-v_1v_2]w + [(d_1+v_1)(d_2+v_2)-v_1v_2]M_2)}{[v_1v_2 - (d_1+v_1-c_1)(d_2+v_2-c_2)]w + [v_1v_2 - (d_1+v_1-c_1)(d_2+v_2)]M_2}.$$
 (45)

On differentiating $x_O(w)$, one finds that

$$\frac{d}{dw}x_O(w) < 0$$

for all parametric values, and therefore,

$$\inf_{w} x_{O}(w) = \lim_{w \to \infty} x_{O}(w)$$

$$= \frac{M_{1} \left[(d_{1} + v_{1})(d_{2} + v_{2} - c_{2}) - v_{1}v_{2} \right]}{\left[v_{1}v_{2} - (d_{1} + v_{1} - c_{1})(d_{2} + v_{2} - c_{2}) \right]}$$
(46)

680

T. DUMRONGPOKAPHAN et al.

and

$$\sup_{w} x_{O}(w) = x_{O}(w)|_{w=0}
= \frac{\left[(d_{1} + v_{1})(d_{2} + v_{2}) - v_{1}v_{2} \right] M_{1}}{\left[v_{1}v_{2} - (d_{1} + v_{1} - c_{1})(d_{2} + v_{2}) \right]}.$$
(47)

In a similar manner, one can find

$$\inf_{w} z_O(w) = \frac{r_1}{\gamma_1 v_1} \left(1 - \sup_{w} x_O(w) \right) \left(M_1(d_1 + v_1) + (d_1 + v_1 - c_1) \sup_{w} x_O(w) \right) \tag{48}$$

and

$$\sup_{w} z_{O}(w) = \frac{r_{1}}{\gamma_{1} \nu_{1}} \left(1 - \inf_{w} x_{O}(w) \right) \left(M_{1}(d_{1} + \nu_{1}) + (d_{1} + \nu_{1} - c_{1}) \inf_{w} x_{O}(w) \right)$$
(49)

provided that (35) holds.

Moreover, we observe that the manifold h=0 intersects the (y,z)-plane along the line given by (36) whose slope is, for a given value of w,

$$\frac{\upsilon_2(w+M_2)}{(d_2+\upsilon_2-c_2)w+(d_2+\upsilon_2)M_2},$$

which has a minimum value when w=0 of $v_2/(d_2+v_2)$. However, the slope of the line where g=0 intersects the (y,z)-plane is found from (32) as $(d_1+v_1)/v_1$. Since

$$(d_1+\upsilon_1)(d_2+\upsilon_2) \ge \upsilon_1\upsilon_2$$

as long as $d_1 > 0$ and $d_2 > 0$, the line where g = 0 intersects the (y, z)-plane is always above the one where h = 0 intersects that plane, as shown in Figure 2a.

The Manifold k=0. This consists of a trivial manifold w=0 and a nontrivial one given by the equation

$$z = \frac{r_2(w + M_2)}{\gamma_2(w + r_3)} \equiv Z_1(w), \tag{50}$$

whose graph is shown projected onto the (w, z)-plane in Figure 3. Since

$$\frac{d}{dw}Z_1(w) = \frac{r_2(r_3 - M_2)}{\gamma_2(w + r_3)^2},$$

which is negative if

$$r_3 < M_2, \tag{51}$$

one finds

and

$$\inf_{w} Z_{1}(w) = \lim_{w \to \infty} Z_{1}(w) = \frac{r_{2}}{\gamma_{2}}.$$
 (53)

We are now in the position to classify the different dynamic behavior exhibited by the system of equations (24)–(27).

CASE 1. This case is identified by inequalities (35), (41), (51), and the separation conditions

$$0 < \inf_{w} x_O(w) \quad \text{and} \quad \sup x_O(w) < x_M, \tag{54}$$

$$0 < \inf_{w} x_{O}(w) \quad \text{and} \quad \sup_{w} x_{O}(w) < x_{M},$$

$$\sup_{w} z_{m}(w) < \inf_{w} Z_{1}(w) \quad \text{and} \quad \sup_{w} Z_{1}(w) < \inf_{w} z_{M}(w),$$
(54)

681

with

$$0 < x_M < \hat{x} < 1, \tag{56}$$

where the infemum and supremum values are as given earlier in (39), (40), (43), (44), and (46)–(49). The inequalities in (54) are the separation conditions required in (16) and (17) of the above theorem, while (55) are those required in (18) and (19). As w varies with time, point O remains between the two stable branches of the curve f = h = 0 and the trajectory will develop into a closed limit cycle, as seen in Figure 2a, which slowly shifts its position with the slowly varying w.

Starting from a generic point, say point A in Figure 2a, a fast transition will develop towards point B on the manifold f=0. Here, g>0 and a transition at intermediate speed will be made in the direction of increasing y until point C on the curve f=g=0 is reached. A slow transition then follows along this curve to point D where the stability will be lost and a catastrophic transition will bring the system to point E on the other stable branch of f=0. Here, g<0 and a transition at intermediate speed will develop in the direction of decreasing y toward point F on the curve f=h=0. A slow transition then follows along f=h=0 until at some point m the stability of the submanifold will be lost. During this time, m will be increasing since m0 here, due to the first inequality in (55). A jump to point m1 followed by a slow transition brings the system to the bifurcation point m2. A catastrophic transition then brings the system to point m3 for the trivial manifold m4 on the trivial manifold m5 of during which time m6 will be decreasing since m6 of here, due to

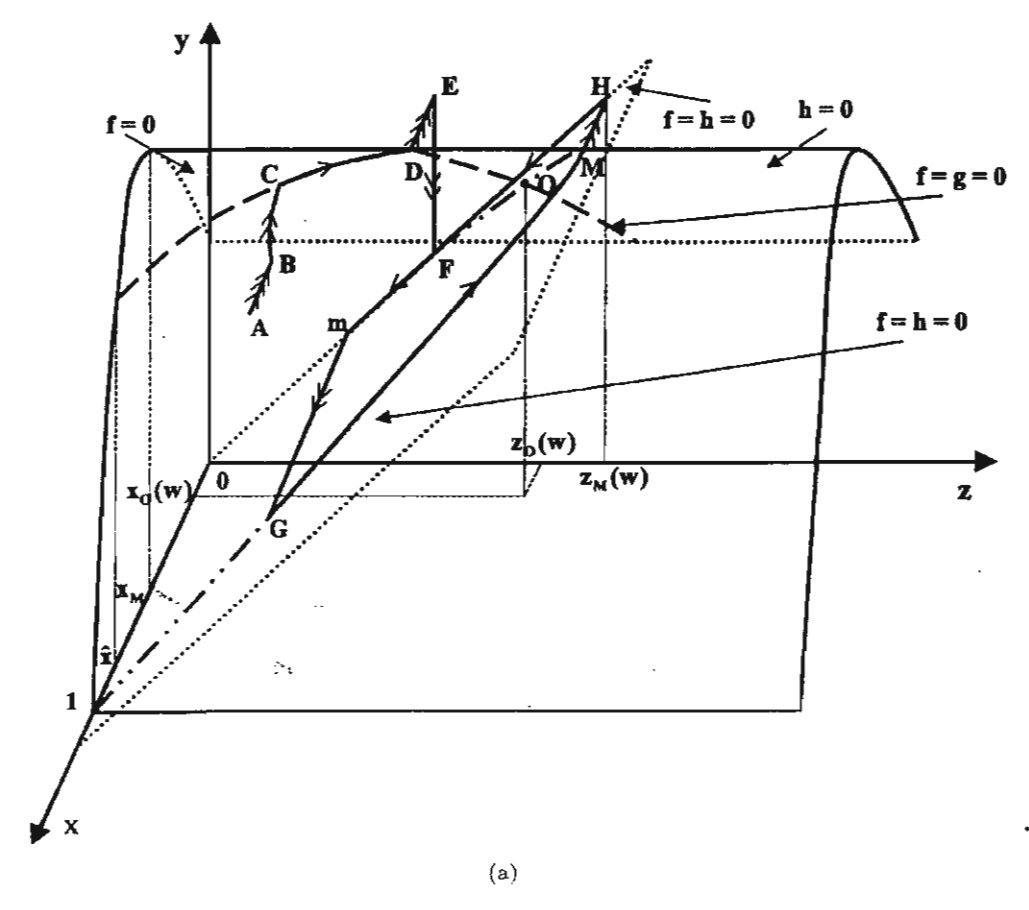
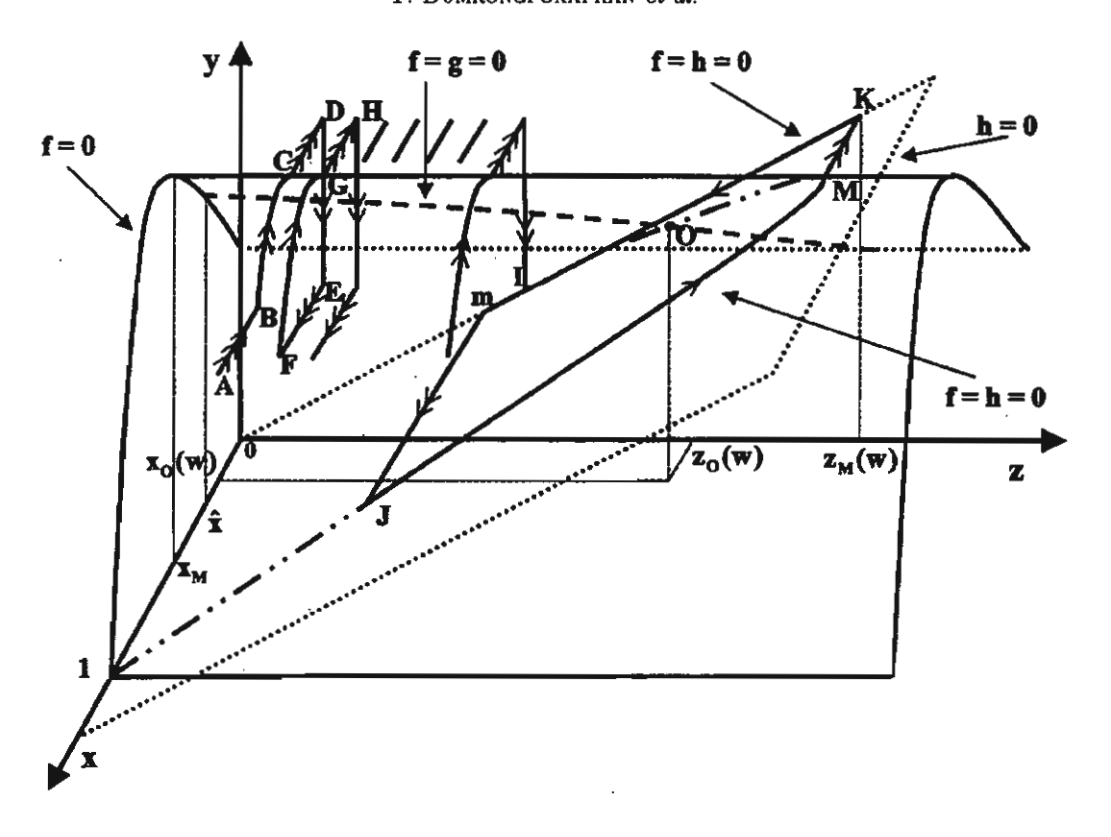
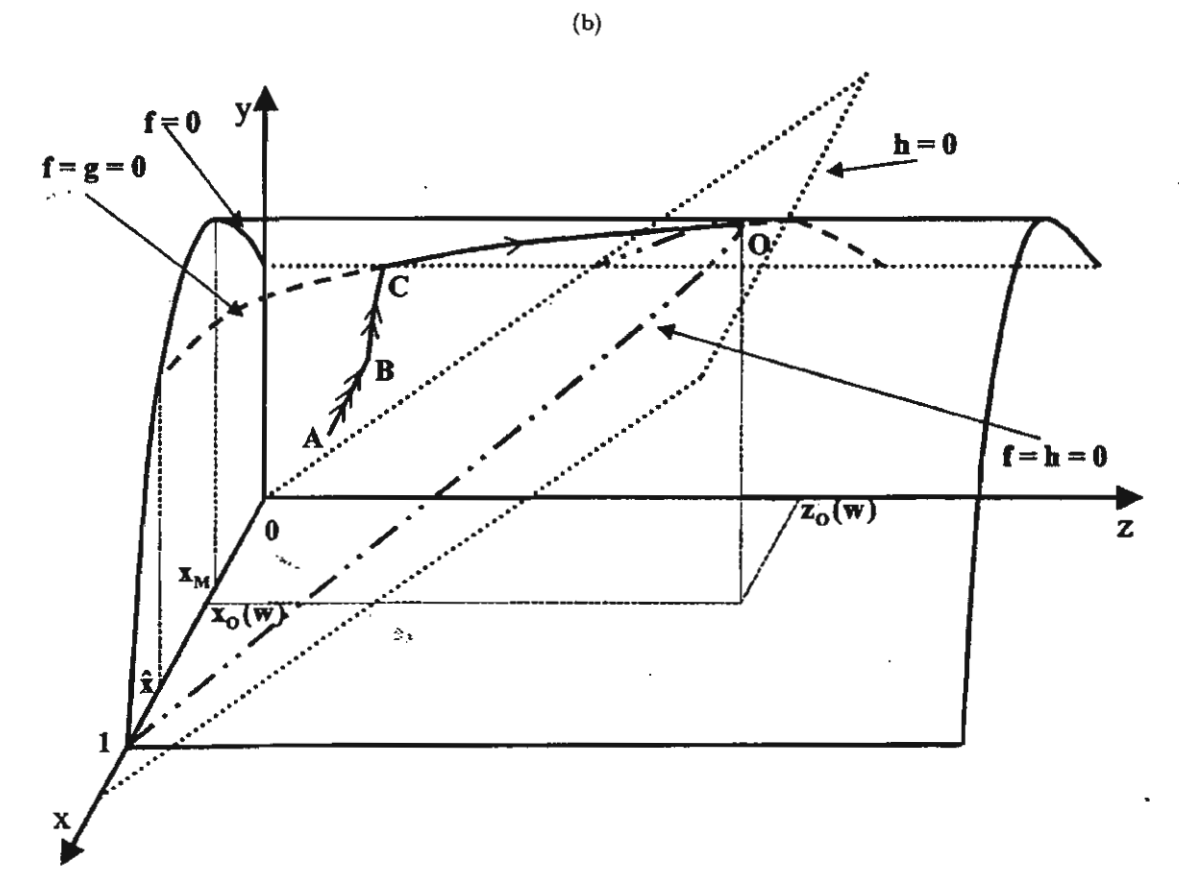


Figure 2. The three equilibrium manifolds f = 0, g = 0, and h = 0 in the (x, y, z)-space for a particular value of w, in the five cases identified in the text. The transitions develop into closed cycles in Figures 2a and 2b, approach the stable equilibrium point O in the positive octant in Figures 2c and 2c, and approach the washout steady state (x, y, z) = (1, 0, 0) in Figure 2d.

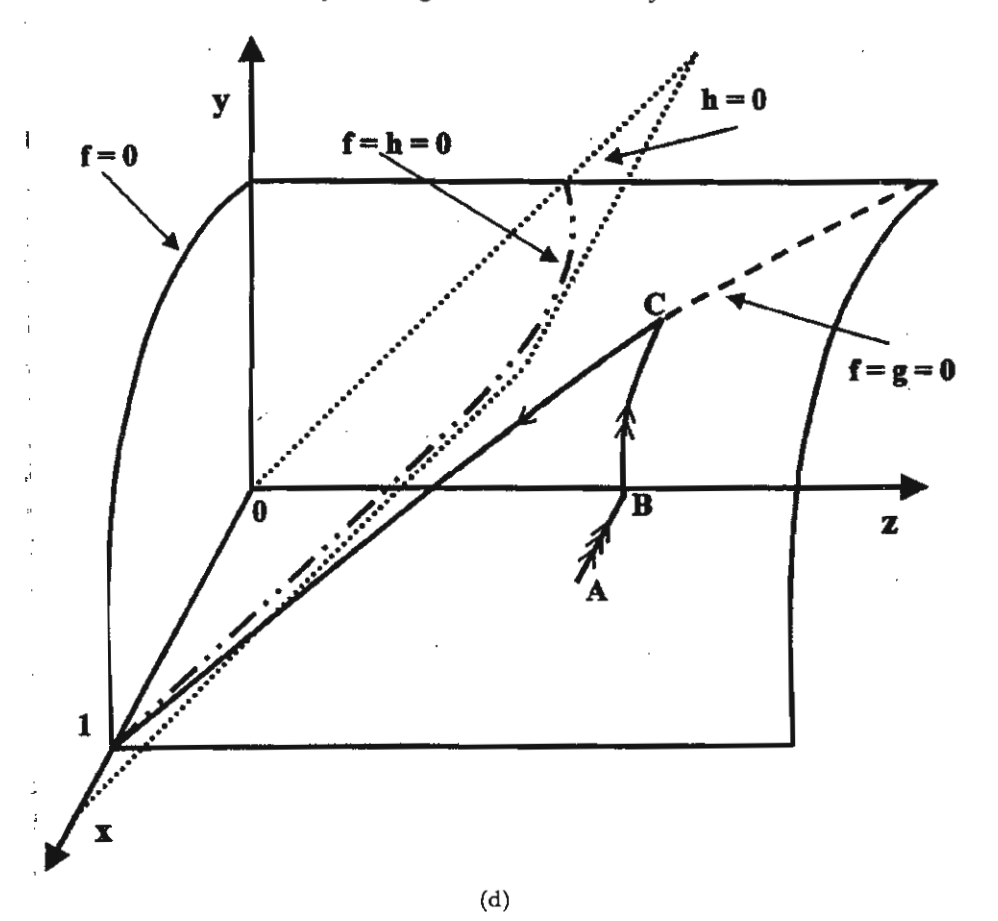
T. DUMRONGPOKAPHAN et al.





(c)

Figure 2. (cont.)



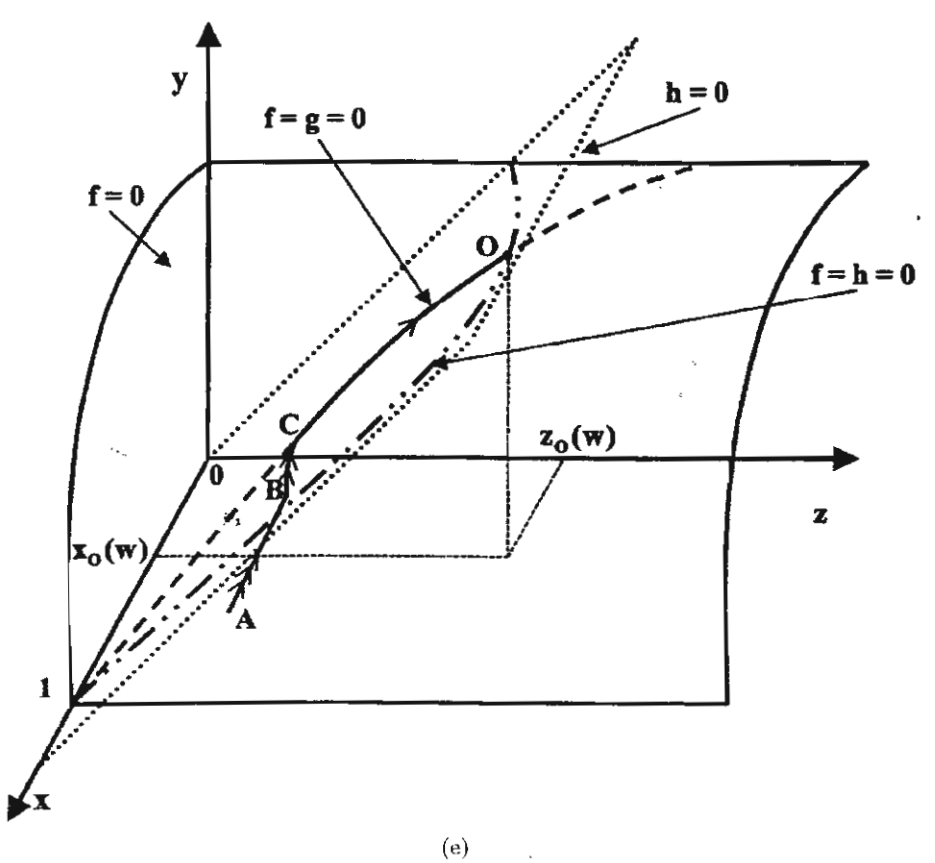


Figure 2. (cont.)

the second inequality in (55). A slow transition will now develop to point m which closes up the cycle mGMHm and thereby a limit cycle has been identified.

CASE 2. In this case, inequalities (35), (41), (51), (54), and (55) still hold, while (56) is now violated and

$$0 < \hat{x} < x_M. \tag{57}$$

The relative positions of the manifolds f = 0, g = 0, and h = 0 are as shown in Figure 2b, slowly shifting with time.

The transition will develop from point A in Figure 2b to B as before. However, a transition at intermediate speed from B will continue upward until the bifurcation point C is reached, where a catastrophic transition will bring the system to point D on the trivial manifold x=0. A transition at intermediate speed follows downward until the stability is lost at some point E and a quick jump takes the system to point E on the other stable branch of E which almost closes up the cycle. However, E has been varying slowly and so point E just misses E and the transition continues upward to point E, then to E and so on, until a point E on the curve E is reached, from which point the transitions will trace out a closed cycle in the same manner as in Case 1.

CASE 3. In this case, inequalities (35), (41), (51), and (56) hold, while the separation condition (54) is violated and we have instead that

$$0 < x_M < \inf_{w} x_O(w). \tag{58}$$

The trajectory will develop as in Case 1, initially. However, since now point O (in Figure 2c) is located on the stable branch of f = 0, the transition from point C on f = g = 0 will first reach point O where f = g = h = 0.

Considering the manifold k = 0 projected onto the (w, z)-plane in Figure 3, we see that w may behave in three different manners. First, if it is further required that

$$\inf_{w} z_O(w) > \sup_{w} Z_1(w) = \frac{r_2 M_2}{\gamma_2 r_3}.$$
 (59)

Then the trajectory eventually stays in the region where $\dot{w} < 0$ and w tends to zero as time passes. Thus, this is the case where the predators can persist on the supply of only one prey pop-

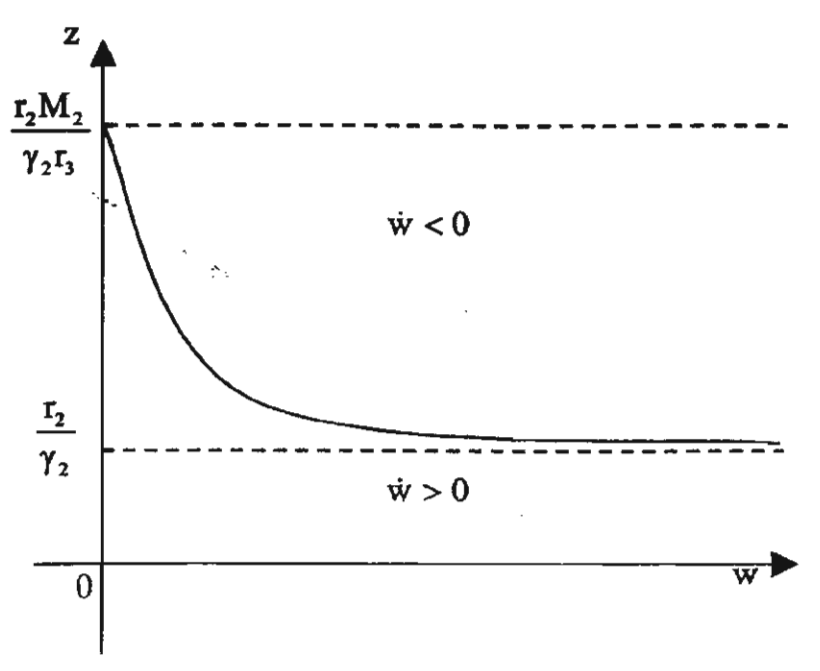


Figure 3. The graph of the manifold k = 0 projected on the (w, z)-plane.

ulation in one community. The mechanism of migration into the other community can be taken as hibernation or fasting periods during which some predators choose abstinence to insure survival. Second, if it is required, on the other hand, that

$$\sup_{w} z_{O}(w) < \inf_{w} Z_{1}(w) = \frac{r_{2}}{\gamma_{2}}, \tag{60}$$

then the trajectory eventually stays in the region where $\dot{w} > 0$ and we will find that w increases unboundedly as time passes.

Finally, if we require

$$\frac{r_2}{\gamma_2} < \inf_{w} z_O(w) \quad \text{and} \quad \sup_{w} z_O(w) < \frac{r_2 M_2}{\gamma_2 r_3}$$
 (61)

instead of inequality (59) or (60), then it is guaranteed that w will tend towards a stable nonzero equilibrium value on the manifold k = 0. This is then the case where all four populations persist at constant levels.

CASE 4. If inequalities (35), (51), and (60) hold, but

$$\hat{x} > 1, \tag{62}$$

then we must have $x_M < 0$ as well, from considering equations (30) and (34). We also note that the curve f = h = 0 can be shown to be concave up, while f = g = 0 is concave down as z increases along the surface f = 0. Therefore, the two curves will not intersect at a point where z > 0 if we make sure that the curve f = h = 0 is steeper than f = g = 0 at the point z = 0, namely, we need to require

$$(M_1+1)(d_1+\nu_1)-c_1>\frac{\nu_1\nu_2(M_1+1)}{d_2+\nu_2}. (63)$$

Then, the three manifolds are positioned as shown in Figure 2d and the transitions will develop from the starting point A to point C on f=g=0 as before. Here, however, h<0 and so a slow transition will develop downward in the direction of decreasing z to end at the equilibrium point (x,y,z)=(1,0,0) where f=g=h=0. Thus, in this case the predator populations vanish in both communities. Prey in the first community eventually reaches the steady level 1, and prey in the second one increases unboundedly since $\dot{w}>0$ once z=0.

CASE 5. On the other hand, if, apart from (35), (51), and (62), we also have

$$(M_1+1)(d_1+\upsilon_1)-c_1<\frac{\upsilon_1\upsilon_2(M_1+1)}{d_2+\upsilon_2},$$
(64)

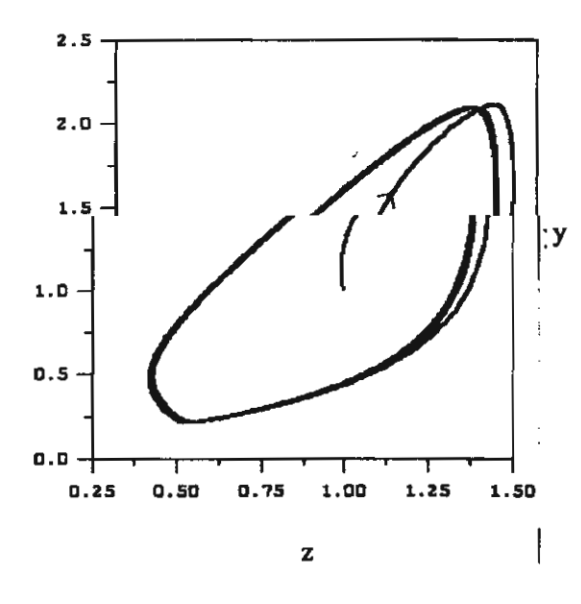
then the curve f = g = 0 is steeper than f = h = 0 at the point z = 0, and they will intersect at some point where z > 0 as shown in Figure 2c. The trajectory will, therefore, develop in the same manner as in Case 3: The populations x, y, and z tend toward steady positive levels, while w either vanishes, establishes a positive constant level, or becomes unbounded, depending on whether inequality (59), (60), or (61) holds, respectively.

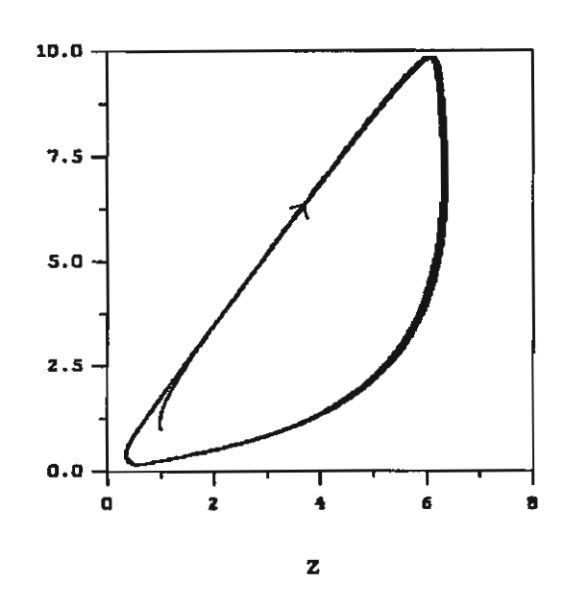
DISCUSSION AND CONCLUSION

We present, in Figure 4, a computer simulation of system (24)–(27) with parametric values chosen to satisfy the delineating conditions in Cases 1–5 described above. Figures 4a–4e show the solution trajectories projected onto the (z, y)-plane, corresponding to Cases 1–5, identified earlier, respectively. The numerical results are in agreement with our theoretical predictions.

Figure 5 shows the corresponding time courses of the state variables in each of the five cases shown in Figure 4. The population levels are seen to develop into sustained oscillations in Cases 1

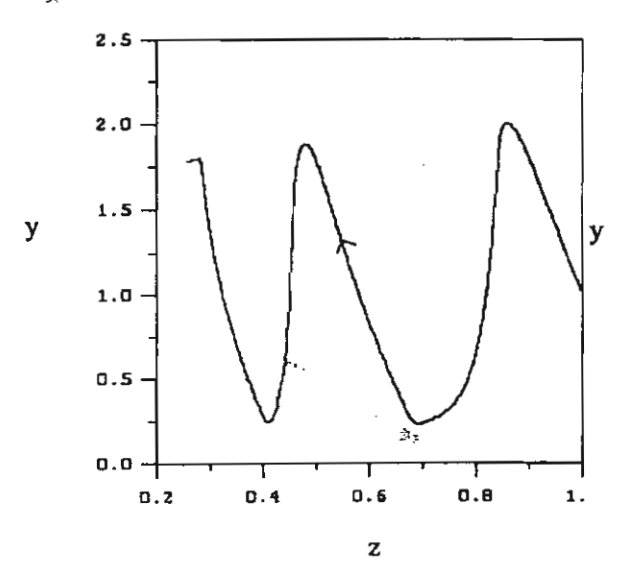
and 2 (Figures 5a and 5b, respectively), and tend toward steady-state levels in Cases 3 and 5 (Figures 5c and 5e, respectively). Case 5 is shown here with (60) being satisfied and all four populations persist, while Case 3 is shown here with inequality (59) being satisfied, and only the first three populations persist, while prey in the second community becomes extinct eventually. Inequality (59) may be interpreted to say that even the lowest value of z_O , the level of predators in the second community, at the point where f = g = 0, below which the levels of both predators

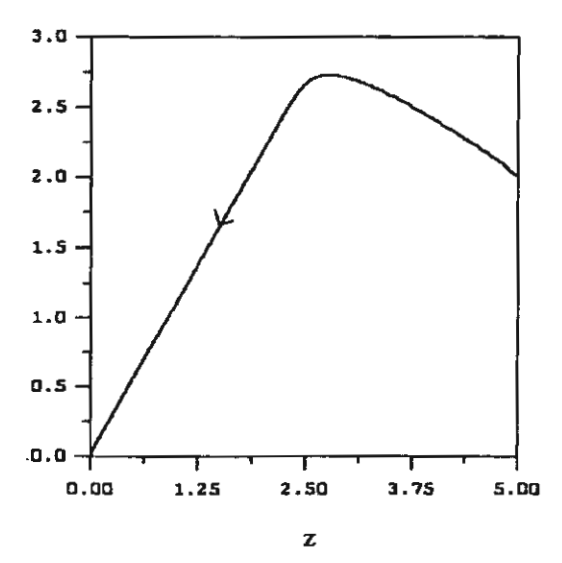




(a) $c_1 = 0.8$, $c_2 = 0.075$, $d_1 = 0.5$, $d_2 = 0.3$, $\gamma_1 = 1$, $\gamma_2 = 3$, $M_1 = 0.1$, $M_2 = 2$, $r_1 = 6$, $r_2 = 2$, $r_3 = 1$, $v_1 = 0.2$, $v_2 = 2$, $\varepsilon = 1$, $\delta = 0.1$, $\eta = 0.5$, x(0) = 1.2, y(0) = 1, z(0) = 1, and w(0) = 1.

(b) $c_1 = 0.7$, $c_2 = 0.1$, $d_1 = 0.5$, $d_2 = 0.3$, $\gamma_1 = 0.2$, $\gamma_2 = 1$, $M_1 = 0.05$, $M_2 = 3$, $r_1 = 6$, $r_2 = 2$, $r_3 = 2$, $v_1 = 0.1$, $v_2 = 2$, $\varepsilon = 1$, $\delta = 0.1$, $\eta = 0.5$, x(0) = 1.2, y(0) = 1, z(0) = 1, and w(0) = 1.

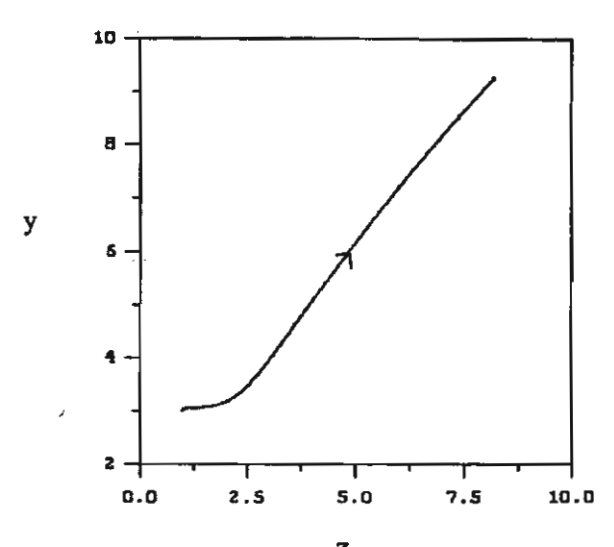




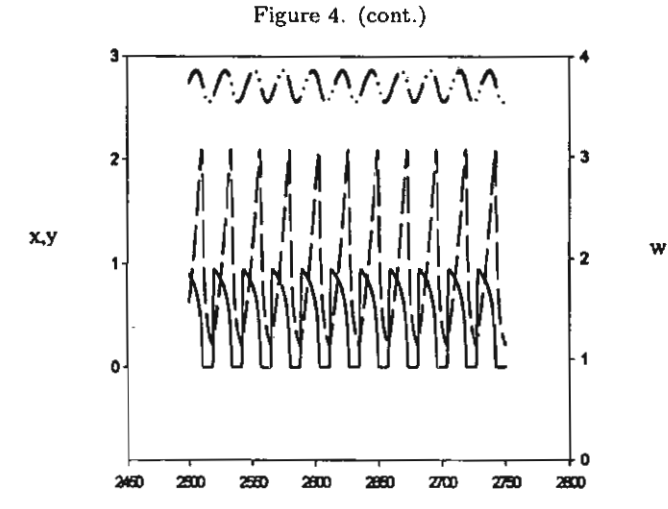
(c) $c_1 = 0.8$, $c_2 = 0.075$, $d_1 = 0.5$, $d_2 = 0.3$, $\gamma_1 = 1$, $\gamma_2 = 3$, $M_1 = 0.1$, $M_2 = 2$, $r_1 = 6$, $r_2 = 0.3$, $r_3 = 1$, $v_1 = 0.2$, $v_2 = 0.05$, $\epsilon = 1$, $\delta = 0.1$, $\eta = 0.5$, x(0) = 1.2, y(0) = 1, z(0) = 1, and w(0) = 1.

(d) $c_1=0.43,\ c_2=0.075,\ d_1=0.1,\ d_2=0.3,\ \gamma_1=1,\ \gamma_2=3,\ M_1=3,\ M_2=8,\ r_1=6,\ r_2=15,\ r_3=1,\ \upsilon_1=0.1,\ \upsilon_2=2,\ \varepsilon=1,\ \delta=0.1,\ \eta=0.5,\ x(0)=2,\ y(0)=2,\ z(0)=5,\ {\rm and}\ w(0)=1.$

Figure 4. Computer simulations of the model equations (26)-(29) in the five cases mentioned in Figure 2. The simulation results agree with our theoretical prediction set out in Figure 2.



(e) $c_1=0.7,\ c_2=0.075,\ d_1=0.1,\ d_2=0.3,\ \gamma_1=1,\ \gamma_2=3,\ M_1=3,\ M_2=8,\ r_1=6,\ r_2=15,\ r_3=1,\ v_1=0.1,\ v_2=2,\ \varepsilon=1,\ \delta=0.1,\ \eta=0.5,\ x(0)=2,\ y(0)=3,\ z(0)=1,\ {\rm and}\ w(0)=1.$



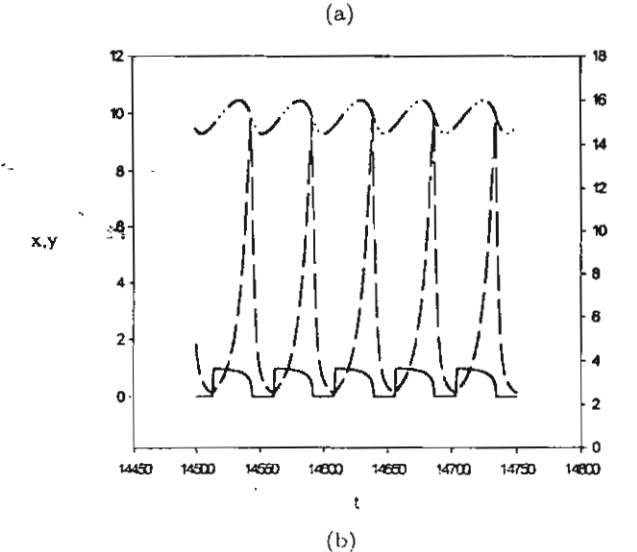
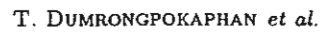


Figure 5. The time courses of three populations $\pi(t)$, y(t), and w(t) in the corresponding five cases shown in Figure 4.



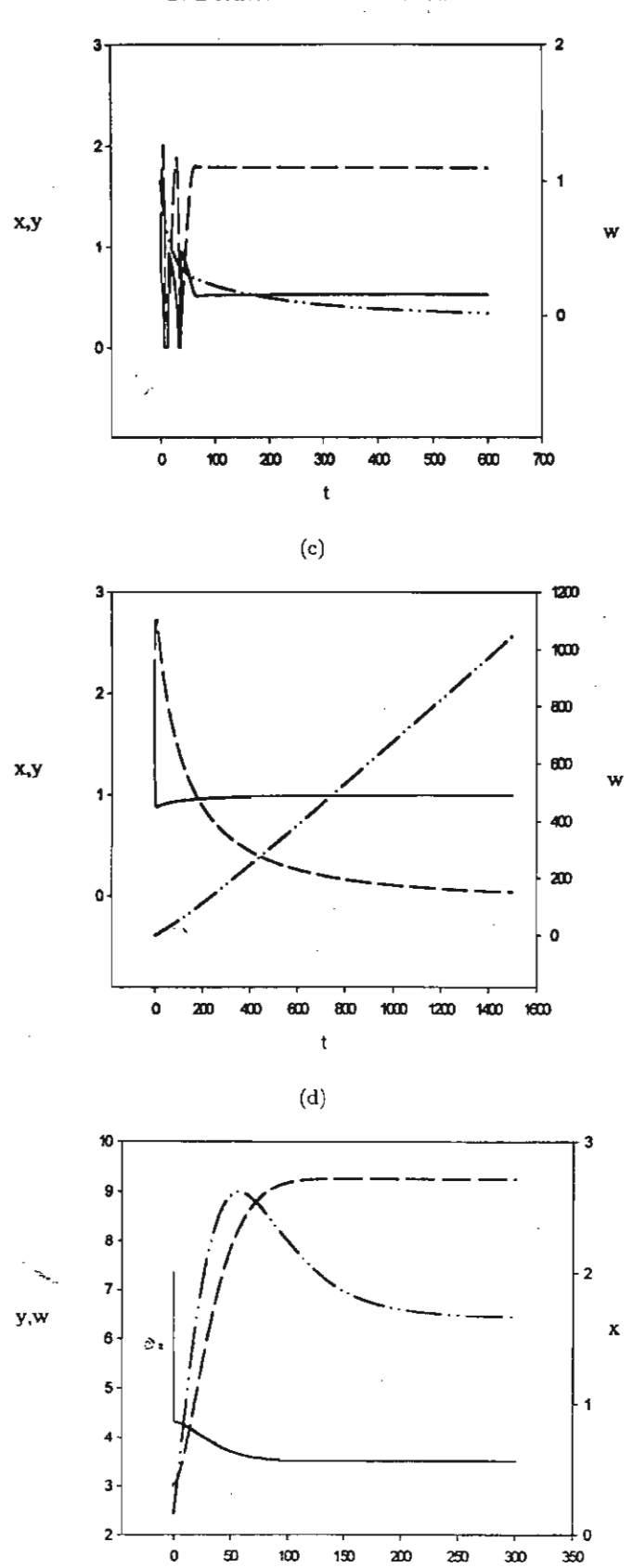


Figure 5. (cont.)

(e)

t

must be rising, is still too high to be sustainable by the preys in the second community, whose slow dynamics then drive them to extinction. Thus, to ensure survival in this case, some predators migrate out of the community or, equivalently, escape into hibernation when sustenance is low in that community.

The separation conditions in (54) for sustained oscillation may be interpreted as follows. The value y_M is the highest possible level of predators in the first community, above which the level of prey x in that community must decline (f < 0). On the other hand, y_O is the level of predators, at the point where f = g = h = 0, above which the levels of prey x and predators y must decline while z begins to rise. The level x_M of prey in the first community, which sustains the first event, must be high enough to exceed the level x_O , which sustains the latter, over all levels of prey w in the second community. The first inequality in (55) may be interpreted as follows. The value $Z_1(w)$ is the level of predators in the second community below which the level of prey w must rise (k > 0). On the other hand, $z_m(w)$ is the level of predators in the second community below which its level must begin to rise when there is no prey in the first community (x = 0). The levels of Z_1 , over all w, must exceed the levels of z_m over all w. A similar interpretation can be made of the second inequality in (55).

Moreover, the requirement that $Z_1(w)$ is bounded above simply means that there should be an upper bound for the levels of predators above which the prey population density in the second community must begin to decline $(\dot{w} < 0)$. Similarly, the condition that $Z_1(w)$ should be bounded below by a positive number means that there must be a positive level of predators below which point the prey population density, whatever it is, must be increasing $(\dot{w} > 0)$.

If the requirements stated above are satisfied, then the surrounding conditions are suitable for sustained oscillations in all four persisting populations. Field data which exhibits oscillatory behavior in connection with migration have often been reported [9,10].

We further note that extinction of predators in both communities is discovered in this system in Case 4 when $\hat{x} > 1$ and (63) holds as presented in Figure 5d. Considering the value of \hat{x} given by (34), \hat{x} will be less than one if

$$d_1 + \upsilon_1 < \frac{c_1}{M_1 + 1}. (65)$$

This means that, to keep from extinction, the predators in the first community must keep the death and migration rates from being too high.

On the other hand, for persistence and stability in the case that $\hat{x} < 1$, we need inequality (41) to hold for the existence of a positive attractor to be assured. This inequality can be satisfied if the migration constant v_2 is large enough while the death rate d_2 can still be low. Thus, migration must be balanced in a proper way to achieve sustainability. In the case that $v_1 = v_2 = v$, then (41) and (65) lead to the requirement that

$$c_2 - d_2 < v < \frac{c_1 - d_1(M_1 + 1)}{M_1 + 1},$$

which gives the bounds for the migration rate v to keep the populations from extinction.

We have, thus, demonstrated the crucial role of migration, variation in reproductive rates, foraging success, and mortality as a mechanism which effects population survival, by the application of the higher-dimensional separation conditions, which in this case pivots about the slow component. Field data has been reported [7,11] which strongly suggests that increasing the number of interacting population, and thus, migration rates, slows down the tendency to extinction. In trying to model such a multipopulated system, the separation conditions can then become more complex. There are several sophisticated computer programs, however, which can render the calculations of bounds and parametric values easy to accomplished. Studies of several other cascade systems may be undertaken through similar analyses which invariably yield valuable insights into the systems under sindy.

T. DUMRONGPOKAPHAN et al.

REFERENCES

- 1. A.W. Norman and G. Litwack, Hormones, Second Edition, pp. 8-9, Academic Press, San Diego, CA, (1997).
- S. Muratori and S. Rinaldi, Low- and high-frequency oscillations in three-dimensional food chain systems, Siam J. Appl. Math. 52, 1688-1706, (1992).
- S. Muratori and S. Rinaldi, A separation condition for the existence of limit cycles in slow-fast systems, Appl. Math. Modelling 15, 312-318, (1991).
- Y. Lenbury, R. Ouncharoen and N. Tumrasvin, Higher dimensional separation principle for the analysis
 of relaxation oscillations in nonliner systems: Application to a model of HIV infection, IMA Journal of
 Mathematics Applied in Medicine and Biology 17, 243-261, (2000).
- 5. H. Matsumoto and H. Seno, On predator invasion into multi-patchy environment of two kinds of patches, *Ecological Modelling* 79, 131-147, (1995).
- H. Whitehead, Variation in the feeding success of sperm whales: Temporal scale, spatial scale and relationship to migrations, Journal of Animal Ecology 65, 429-438, (1996).
- S.J. Walde, Immigration and the dynamics of a predator-prey interaction in biological control, Journal of Animal Ecology 63, 337-346, (1994).
- 8. T.W. Sherry and R.T. Holmes, Winter habitat quality, population limitation, and conservation of neotropical-nerctic migrant birds, *Ecology* 77, 36-48, (1996).
- 9. F.J. Ebling, A.D. Hawkins, J.A. Kitching, L. Muntz and V.M. Pratt, The ecology of Lough Ine XVI. Predation and diurnal migration in the paracentrotus community, *Journal of Animal Ecology* 35, 559-566, (1966).
- 10. J.E. Diffendorfer, M.S. Gaines and R.D. Holt, Habitat fragmentation and movements of three small mammals (sigmodon, microtus, and peromyscus), *Ecology* 73, 827-839, (1995).
- 11. B.W. Dale, L.G. Adams and R.T. Bowyer, Functional response of wolves preying on barren-ground caribou in a multiple-prey ecosystem, *Journal of Animal Ecology* 63, 644-652, (1994).

ů,



Available online at www.sciencedirect.com

J. Math. Anal. Appl. 305 (2005) 631-643

Journal of
MATHEMATICAL
ANALYSIS AND
APPLICATIONS

www.elsevier.com/locate/jmaa

Delay effect in models of population growth

Dang Vu Giang a, Yongwimon Lenbury b,*, Thomas I. Seidman c

^a Hanoi Institute of Mathematics, 18 Hoang Quoc Viet, 10307 Hanoi, Viet Nam
^b Department of Mathematics, Faculty of Science, Mahidol University, Rama 6 Road,

Bangkok 10400, Thailand

^c Department of Mathematics and Statistics, University of Maryland Baltimore County,
Baltimore, MD 21250, USA

Received 29 June 2004

Available online 20 January 2005

Submitted by P.G.L. Leach

Abstract

First, we systematize earlier results on the global stability of the model $\dot{x} + \mu x = f(x(\cdot - \tau))$ of population growth. Second, we investigate the effect of delay on the asymptotic behavior when the nonlinearity f is a unimodal function. Our results can be applied to several population models [Elements of Mathematical Ecology, 2001 [7]; Appl. Anal. 43 (1992) 109–124; Math. Comput. Modelling, in press; Funkt. Biol. Med. 256 (1982) 156–164; Math. Comput. Modelling 35 (2002) 719–731; Mat. Stos. 6 (1976) 25–40] because the function f does not need to be monotone or differentiable. Specifically, our results generalize earlier result of [Delay Differential Equations with Applications in Population Dynamics, 1993], since our function f may not be differentiable. © 2004 Elsevier Inc. All rights reserved.

Keywords: Delay differential equations; Comparison theorem; ω-limit set of a persistent solution; One-parameter semi-group; Convergence to equilibrium; Nicholson's blowfly model; Periodic solutions

^{*} Corresponding author.

E-mail addresses: dangvugiang@yahoo.com (D.V. Giang), scylb@mucc.mahidol.ac.th (Y. Lenbury), seidman@math.umbc.edu (T.I. Seidman).

 ⁰⁰²²⁻²⁴⁷X/\$ – see front matter © 2004 Elsevier Inc. All rights reserved. doi:10.1016/j.jmaa.2004.12.018

1. Introduction

Given a continuous function $f: \mathbb{R}_+ \to \mathbb{R}_+$ and a nonnegative function $\xi \neq 0$ on $[-\tau, 0]$, we consider the delay differential equation

$$\dot{x} + \mu x = f(x(\cdot - \tau)), \qquad x(s) = \xi(s) \quad \text{for } s \in [-\tau, 0]. \tag{1.1}$$

For simplicity, we assume throughout that ξ is bounded. It follows that (1.1) has a unique solution—e.g., one can proceed by intervals of length τ —with $x_{f,\xi}(\cdot)$ nonnegative and continuous for $t \ge 0$. We denote the solution of the delay differential equation (1.1) by $x(\cdot) = x_{f,\xi}(\cdot)$. It is easily seen that one has the equivalent integrated formulation:

$$x(t) = e^{-\mu(t-a)}x(a) + \int_{a}^{t} e^{-\mu(t-s)} f(x(s-\tau)) ds$$
 (1.2)

for $t \ge 0$. (Actually, continuity of f is not needed for (1.2), only enough regularity to ensure the requisite integrability.) We further note the following

Lemma 1. Given real constants μ , ν and $\tau > 0$, there is a function X = X(t) such that the solution y of the autonomous linear delay differential equation

$$\dot{y} + \mu y + \nu y(t - \tau) = g(t), \quad y|_{[-\tau,0]} = \eta,$$
 (1.3)

has the integral representation

$$y(t) = y_0(t; \eta) + \int_0^t X(t - s)g(s) ds,$$
 (1.4)

where $y_0 = y_0(\cdot; \eta)$ is the solution of the associated homogeneous initial value problem. Both $X(\cdot)$ and y_0 decay exponentially if

$$h(z) := z + \mu + \nu e^{-\tau z} = 0 \quad \Rightarrow \quad \Re(z) < 0,$$
 (1.5)

i.e., if every root of the characteristic equation has (strictly) negative real part, and grow exponentially if $h(\cdot)$ has any root with positive real part.

Proof. See, e.g., [6]. Note that

$$||X||_1 = \int_0^\infty |X(t)| dt < \infty \tag{1.6}$$

when X decays exponentially. \square

A standard calculation shows that (1.5) holds for all $\tau > 0$ when $|\nu| < \mu$ and, conversely, fails when $|\nu| > \mu$ unless τ is restricted so that

$$\tau < \tau_* = \tau_*(\mu, \nu) = \frac{\arccos[-\mu/\nu]}{\sqrt{\nu^2 - \mu^2}}$$
 (1.7)